INSTITUTO SUPERIOR DE ENGENHARIA DE LISBOA

Área Departamental de Engenharia Electrotécnica Energia e Automação

OSCILLATING DRIVING CIRCUIT FOR A WIRELESS POWER TRANSFER SYSTEM

Thesis presented for the Master's Degree in Electrical Engineering

Miguel Filipe Matos de Rhodes

February 2017

MASTER SURPEVISORS:
DOUTOR LUÍS MANUEL DOS SANTOS REDONDO
DOUTOR MIGUEL CABRAL FERREIRA CHAVES

JÚRY:
PRESIDENT: PROFª.ADJ. MARIA DA GRAÇA ALMEIDA

VOGAIS: MARCOS TEOTÔNIO PEREIRA

Abstract

In this thesis a power converter is designed to power a wireless power transfer system. The Converter is composed by a DC-AC Class-E inverter, a matching circuit and a spiral antenna. The system is designed to provide 200W and has a working frequency of 13.57 MHz, to comply with the restriction of the radio regulations. Other solutions and the reason for the choice are presented. the theory of modes is briefly introduced characterize a wireless power transfer system.

The components of the Class-E inverter were calculated to guarantee the Zero Voltage Switching (ZVS) operation, resulting in the only losses in the system been the conducting ones. When operating in optimal conditions, the converter has an efficiency higher than 90%.

A spiral Antenna is designed and its self-inductance is calculated utilizing potential vectors. The antenna has the purpose of exciting the wireless power transfer system. To attach the antenna to the inverter a matching circuit is designed to make sure that the inverter operates with high efficiency, regardless of the antenna's impedance.

The results were provide by simulations using Orcad's PSpice software and the components calculations were made using MATLAB. The simulation results show the behavior of the system working in non-optimum conditions and they are used to tune the components of the inverter and the matching circuit to achieve ZVS on the MOSFET and reach the highest efficiency.

Keywords

Wireless Power Transfer, Class-E Inverter, ZVS, Mode Theory;

Resumo

Nesta tese um um conversor de potência é desenvolvido com o objetivo de alimentar um sistema de transferência de energia sem fios. O conversor é composto por um inversor Class-E, um circuito adaptativo e uma antena espiral. O sistem é dimensionado para fornecer 200W e opera a uma frequência de 13,57 MHz, obedecendo os regulamento da leis internacionais de transmissão de radio. A teoria dos modos é brevemente introduzida para caracterizar um sistema de transferência de energia sem fios.

Os componentes do inversor Class-E foram calculados para garantir o funcionamento em ZVS (Zero voltage Switching), portanto a unicas perdas são as perdas de condução. Quando operando nas condições ótimas de funcionamento, o inversor tem uma eficiência acima dos 90%.

A antena espiral é dimensionada e sua auto-indutancia é calculada com vetores potênciais. O propósito da antena é excitar o sistema de transferência de energia sem fios. Para juntar a antena e o inversor, um sistema adaptativo é desenvolvido para compensar a mudança de impedancia causada pela antena. Dessa forma, o circuito pode operar na sua eficiência máxima.

Os resultados foram obtidos por simulações utilizando PSpice, da Orcad, e os componentes foram calculados com MATLAB. As simulações mostram o funcionamento quando o sistema não opera no modo ótimo e como é possivel afinar os componentes do inversor e o cirucito adaptativo para atingir o ZVS no MOSFET e manter a eficiência alta.

Palavras-Chave

Transferência de potência sem fios, Inversor Class-E, ZVS, Teoria dos Modos;

Acknowledgments

I would like to thank my dissertation supervisor Prof. Luís Redondo, Ph.D., for taking this challenge at short notice and support me with his guidance, experience, insight and resources. Having working with him made me always work harder and look for the better and more complete solution and that definitively raised my quality as an engineer.

I would also like to thank Prof. Miguel Chaves, Ph.D., for always being available to help me no matter what the issue was. His insights added great value to this work.

I am grateful for Prof. João Cassaleiro and Prof. Carlos Mendes, both Ph.D., for helping me with issues beyond my area of knowledge. Their willingness to help made this work possible.

I would like to thank my colleagues and friends Sérgio André and Alexandre Bento for their help, friendship, being by my side during many hours of work and for making big problems seem small.

I am also grateful to all my Portuguese friends for making me feel always at home in Portugal

I'm very grateful to my lovely girlfriend Maria São Pedro for her unending patience and carrying. Her ability to push me beyond my limits made me overcome all challenges.

I owe my deepest gratitude to my parents, Marly Rosa and Filipe Rhodes, and my grandmother, Maria Julia Rhodes, for providing all my life their immeasurable support, wisdom and love. Without them, I would not be where I am today.

Symbol Table

L	Resonant Tank Inductance [H]
C	Resonant Tank Capacitor [F]
R_i	Class-E Inverter AC Load [Ω]
C_1	Class-E Inverter Shunt Capacitor [F]
L_f	Class-E Inverter Choke Inductance [H]
V_I	Direct Current Source [V]
v_s	Voltage Across the Switch [V]
$\frac{dv_s}{d_t}$	The variation of the Switch Voltage in Time [V/s]
C_{eq}	Equivalent Capacitance resulting from parallel of C and C_1[F]
ω	Working Angular Frequency [rad/s]
f	Working Frequency [Hz]
f_{01}	Resonant Frequency of Normal Series-Resonant Circuit [Hz]
f_{02}	Resonant Frequency o Series-Resonant Circuit with Shunt Capacitor [Hz]
Q_L	Quality Factor
D	Duty Cycle
f	Working Frequency [Hz]
I_I	Source Current [A]
i_s	Switch Current [A]

i_{C1}	Shunt Capacitor Current [A]
i	Resonant Tank Current [A]
L_a	Inductance at Resonance Frequency [H]
L_b	Representative Load Inductance when Load is at Working Frequency [H]
I_m	Resonant Tank Current Amplitude [A]
ϕ	Load Current Phase [º]
v_{L_i}	Voltage across Inductance at Working Frequency [V]
$V_{R_{im}}$	Voltage Amplitude across Load at Working Frequency Amplitude [V]
$I_{R_{im}}$	Current Amplitude across Load at Working Frequency Amplitude [A]
$V_{L_{im}}$	Voltage across Inductance at Working Frequency Amplitude [V]
$V_{R_{im}}$	Voltage across Load at Working Frequency Amplitude [V]
v_{R_1}	Total Resonant Tank Voltage at Working Frequency [V]
$V_{R_{m1}}$	Resonant Tank Voltage at Working Frequency Amplitude [V]
ψ	Phase Between Load Voltage and Total Resonant Tank Voltage [º]
P_{Ri}	Load Power [W]
R_{DC}	Class-E Inverter Resistance, viewed from the Source [Ω]
$V_{L_{bm}}$	Voltage across Inductance Load at Working Frequency Amplitude [V]

V_{sm}	Voltage Amplitude across the Switch [V]
v_{GS}	Gate Voltage [V]
f_{a1}	Transmitter Antenna's Self-Resonant Frequency [Hz]
C_{a1}	Transmitter Antenna's Parasitic Capacitance [F]
L_{a1}	Transmitter Antenna's Total Inductance [H]
R_{a1}	Transmitter Antenna's Resistance [Ω]
R_{q1}	Transmitter Dumping Resistance [Ω]
C_{pa1}	Transmitter Antenna's Parallel Equivalent Parasitic Capacitance [F]
L_{pa1}	Transmitter Antenna's Parallel Equivalent Total Inductance [H]
R_{pa1}	Transmitter Antenna's Parallel Equivalent Resistance [Ω]
C_2	Matching Circuit Series Capacitance [F]
C_3	Matching Circuit Parallel Capacitance [F]
$a(t)$	Mode
a	Amplitude Mode
E	Mode Energy
G	Mode Loss Conductance
$\frac{1}{\tau}$	Mode Decay Ratio
P_d	Average Mode Power Loss
k	Coupling Coefficient

$S_m(t)$	Incident Excitation Wave
Q_0	Mode Quality Factor

Abbreviations

$ISMB$	The Industrial, Scientific and Medical Band
RF	Radio Frequency
EMF	Electromagnetic Field
AC	Alternating Current
DC	Direct Current
ZVS	Zero-Voltage-Switching
$MOSFET$	Metal Oxide Semiconductor Field Effect Transistor
RMS	Root Mean Square
EMC	Electromagnetic Compatibility
RMS	Radio Frequency Identification
CMT	Coupled Mode Theory

Contents

Chapter 1 Introduction 1
1.1 Motivation 1
1.2 Objectives 1
1.3 Organization 2
Chapter 2 State of the art 3
2.1 Introduction 3
2.2 Potential 5
2.3 Technology 7
2.3.1 Microwaves 7
2.3.2 Electromagnetic Induction 9
2.3.3 Resonant Coupling + Evanescent Fields 14
2.4 Power Source and Inverters 15
Chapter 3 Coupled Mode Theory and Class-E inverter 18
3.1 Coupled Mode Theory 18
3.1.1 Introduction – The Coupling of Modes 18
3.1.2 Formalism 19
3.1.3 Efficiency 25
3.2 Driver's Circuit 26
3.2.1 Class-E's Operation and Design Specifications 26
3.2.1.1 Components Values 29
3.2.1.2 Resume of the components values equations with D=0.5 35
3.2.2 Matching Circuit 36
3.2.2.1 Introduction 36
3.2.3 Driver's Antenna 37
3.2.3.1 Setting up the Antenna 37
3.2.3.2 – Components Calculations 39
3.2.3.3 Antenna's Inductance Calculation 40
Chapter 4 Simulations, Tuning and Results 42
4.1 Simulation parameters 42
4.1.1 Components calculations and choice 42
4.2 Class-E simulation Results 43

4.3 – Antenna Inductance 47
4.4 – Tuning $\boldsymbol{C2}$ and $\boldsymbol{C3}$ 48
Chapter 5 Conclusions 50
5.1 Final Conclusion 50
5.2 Future Work 51
Appendix 52
Appendix A – Driver's components calculation 52
Appendix B – Antenna's inductance Calculation 54
Appendix C – MOSFET's Datasheet 56
Bibliography 58

List of Figures

Figure 2.1- Apparatus to wireless power transfer 3
Figure 2.2 - In Colorado Springs, a Tesla coil receiver tuned in resonance with a Tesla coil transmitter illuminates a 10-watt incandescent lamp. The distance from the transmitter's ground plate to the point of reception is 591 m 4
Figure 2.3 - high-end cellphones have high performance and need a bigger battery to last as much as a regular cellphone. If not properly designed, catastrophic failures can happen 5
Figure 2.4 – In factories, most tasks can be performed using only one tool, but the workers need charge them during the shifts, so they need two, in order to make the task interrupted. 6
Figure 2.5 - Tesla Model S P100D has the longest distance range with 547 Km in one charge, at in a average speed of 100Km/h and can fast charge in 15-30 minutes [SITE DA TESLA] 6
Figure 2.6 - A possible configuration for the system 8
Figure 2.7 - Concept of surveillance UAV, powered by microwaves 8
Figure 2.8 - A deconstructed electric toothbrush. The coil on the end charges the batteries through induction without been expose 10
Figure 2.9 - A RFID tag 10
Figure 2.10 - A RFID working in the near field can be seen as an air-cored transformer 11
Figure 2.11 - the Tacoma Narrows Bridge collapse is one of the best examples of mechanical resonance. The periodic wind blows matched the natural frequency of the bridge's structure. At resonance, the force from the moviments as enough to make it collapse. 12
Figure 2.12 – From [7], the blue and pink lines represent the power transfer and reflected, respectively. Each graph illustrates a different gap length: (a) = 49 cm, (b) = 80mm, (c) = 170 mm (d) = 357 mm 13
Figure 2.13 - Different matching circuit topologies 13
Figure 2.14 - Experiment from [15] . The coils transferred 60W with a distance of 2 meters 15
Figure 2.15 – Example of inverter made of a bridge of with IGBTs 16
Figure 2.16 – Example of a Class-D inverter 17
Figure 2.17 - Example of a Class-f inverter 17
Figure 3.1 - Wireless power transfer system 18
Figure 3.2 – A regular LC Circuit 19
Figure 3.3 – Conductance represents a loss in the LC circuit 21
Figure 3.4 – The behavious of the modes's energy in time 24
Figure 3.5 - Class-E Inverter 27
Figure 3.6 - Voltage across switch in optimum operation and current across the load with $\boldsymbol{QL \geq 2.5}$ 28

Figure 3.7 – Equivalent circuit of Class-E Inverter working between the two resonance frequencies and its parameters 30
Figure3.8 - Equivalent circuit of the resonant tank working above resonance 31
Figure 3.9 - Phasor diagram of the resonant tank at frequency $\boldsymbol{f0}$ 32
Figure3.10 - Drain-Source voltage waveform with load mismatch ($\boldsymbol{RI = 50\Omega}$) 36
Figure 3.11 – Antenna's Equivalent Circuit 37
Figure 3.12 – Transmitter Antenna with Damping Resistors in each terminal 38
Figure 3.13 – Transmitter Antenna Parallel Equivalent Circuit 39
Figure 3.14 - Transmitter Antenna with Damping Resistors and Matching Circuit 40
Figure 4.1 – Designed Class-E Inverter 43
Figure 4.2 – Drain-Source voltage waveform without tuning $\boldsymbol{C1}$ 44
Figure 4.3 – Drain-Source Voltage with $\boldsymbol{C1 = 1pF}$ 44
Figure 4.4 – Drain-Source Voltage with $\boldsymbol{C1 = 100pF}$ 44
Figure 4.5 – Drain-Source Voltage Waveform with $\boldsymbol{C1}$ Tuned 45
Figure 4.6 - Output Voltage and Current 46
Figure 4.7 – Output Current and Source Current with $\boldsymbol{Lf = 12\mu H}$ 46
Figure 4.8 - Driver's antenna 47
Figure 4.9 - Drain-Source Voltage Waveform with untuned matching circuit; $\boldsymbol{C2 = 55.15}$, $\boldsymbol{C3 = 6pF}$ 48
Figure 4.10 – Example for when the load resistance is out of the limits 48
Figure 4.11 - Drain-Source Voltage Waveform with tuned matching circuit; $\boldsymbol{C2 = 28}$, $\boldsymbol{C3 = 1pF}$ 49
Figure 4.12 – Complete Driver Circuit 49

Chapter 1
Introduction

1.1 Motivation

The world has seen a big evolution in technology in the last two decades. Electronic devices became smaller, powerful and accessible to everyone, making them part of our everyday life. Creative ideas made them very functional, connecting the whole world with cellphones, giving the ability to work virtually everywhere with portable computers, turning factory highly productive and environmentally friendly in industrial settings. As powerful and helpful as they are, all of them have one big flaw: the autonomy.

Most smartphone last less than 24 hours, with moderate usage, before it must be recharged again. Companies invest greatly in on their battery's devices, but it is a recurrence problem. To keep their devices powered, many people carry their charging cable with them. Besides that being inconvenient, they still have to find a power outlet and wait. Another popular solution is powerbanks. While they are helpful in many situations, it is just another device to carry and charge.

In industrial facilities, there is various hazard environments due to flammable materials, where a single spark from a switch or plugging a device to a power outlet can produce explosions or fires. This type of danger would not be a concern, if power would be transmitted without wires and if expose contacts completely remove from such environments.

It's obvious the reasons why is so advantageous of implementing the technology of wireless power transfer and not having to worry about the charge of a device, been it for convenience or safety.

Technology evolved to the point that these gadgets can already be used for communications purposes (phone calls, internet, GPS) wirelessly and the next big step should be to maintain their charge wirelessly as well. Only then, they will become truly autonomous.

1.2 Objectives

This works consists in introducing and briefly explain and define a system capable of power exchange wirelessly between two single loop coils coupled magnetically. In order for this system to work, it will be excited also wireless by a resonant circuit. The focus of this thesis is to present different solutions for the "driver" of the coupled

circuit, to fully explain its theory and operation, calculate the components present on it and analyze the results from the simulations. To achieve this objective, PSpice software will be used to analyze the dynamic and steady state of the circuit and MATLAB to make the necessary calculations.

The whole system can be divided in two parts. The first being the driver circuit, which has the role of creating an oscillating current with a chosen fixed frequency, that will flow through an antenna that will couple with the first loop antenna. The current will be generated by a Class-E inverter, consisting of a RLC circuit, a DC source and a MOSFET. For optimal operation of the inverter, a matching circuit will also be developed to reduce the losses in the MOSFET and generate the magnetic field as efficient as possible. The second part is the coupled resonant system, consisting of the two loop antennas magnetically coupled and a small load linked to the second loop antenna through magnetic coupling. This part will not be deeply explained, but it will be introduced the conditions for the system to be in the called "Strong coupled regime" and how it improves the energy exchange through an evanescent field coupling.

1.3 Organization

This thesis has 5 chapters and 2 appendixes, as seen in the contents.

Chapter 1 presents a brief introduction to the wireless power transfer, including the motivation for this thesis, the objectives and how the work is organized.

Chapter 2 is about the state of the art of the technology for wireless power transfer. It will be presented a brief history, different methods and its vantages and disadvantages. Projects already made will be analyzed and the innovations made pointed out. Suggestions of applications and its specifications are also shown here.

Chapter 3 is reserved to the theory of Coupled modes, circuit analysis, circuit topologies and the explanation of the specification used to design the system, such frequency band, power, load values etc. A meticulous explanation of all the sub-system that make the drive's circuit are made here.

Chapter 4 shows the results of the PSpice simulations, the analysis of it and the tuning of the matching circuit.

In chapter 5 conclusions are presented and suggestions for future work

Chapter 2
State of the art

2.1 Introduction

Wireless power transfer is not a new idea. In 1900, Inventor and scientist Nikola Tesla had published a patent about an apparatus, figure 2.1, capable of transmitting electric energy to others devices through the air, without any kind of wires [1].

In the patent filled from Dr. Nikola Tesla [1], it reads:

"It will be readily understood that when the above-prescribed relations exist the best conditions for resonance between the transmitting and receiving circuits are attained, and owing to the fact that the points of highest potential in the coils or conductors A A' are coincident with the elevated terminals the maximum flow of current will take place in the two coils, and this, further, necessarily implies that the capacity and inductance in each of the circuits have such values as to secure the most perfect condition of synchronism with the impressed oscillations"

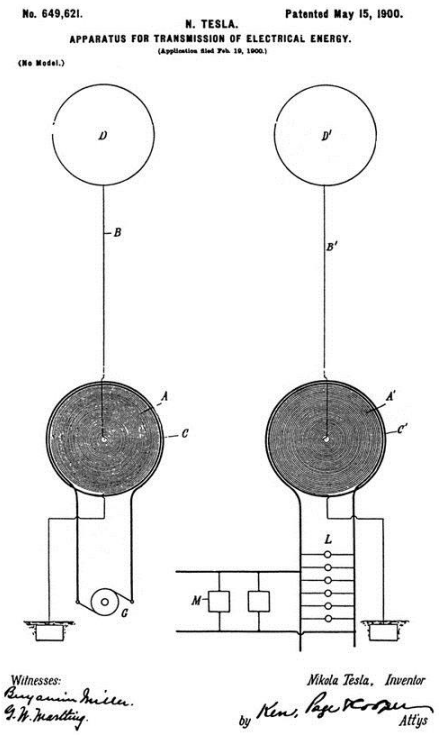

Figure 2.1- Apparatus to wireless power transfer

The Tesla Coil is an example of wireless energy transfer. The primary and secondary coil are a LC circuit, which are not connected by any means, except by magnetic coupling. The primary coil charges the capacitor in the secondary coil. The efficiency of this energy exchange is greatly improve when the two circuits are in magnetic resonance. The whole system works very much as an air-cored transformer, with the secondary coil inside the primary coil. The ambition of Dr. Tesla to transport electric AC power worldwide led him to test the earth as a conducting mean to also transfer power. He increased the scale of the Tesla Coil (this bigger Tesla Coil was called the magnifying transmitter) to discharge lighting strikes up to 3.5MV to the ground to emit energy to receiver (figure 2.2) far in distance.

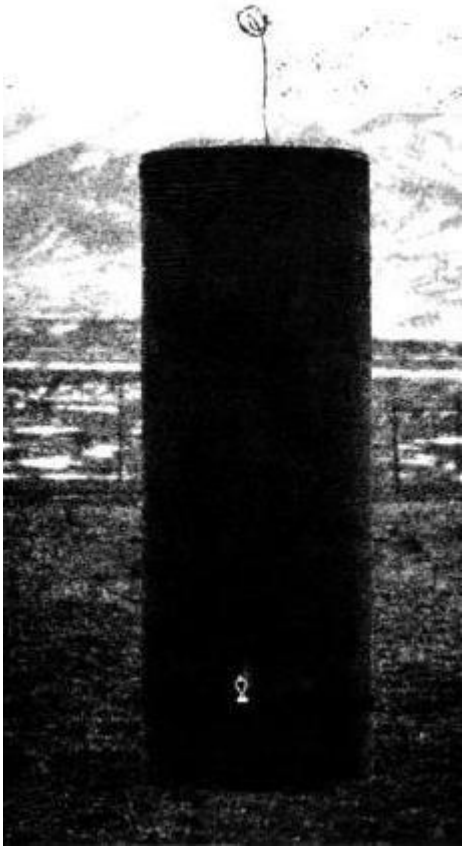

Figure 2.2 - In Colorado Springs, a Tesla coil receiver tuned in resonance with a Tesla coil transmitter illuminates a 10-watt incandescent lamp. The distance from the transmitter's ground plate to the point of reception is 591 m

These experiments showed that it was possible to transmit energy without the need of using wires, as Dr. Tesla envisioned, however the lack of funds from investors and the apprehension from the general population led the study and implementation of those ideas to never be fully put into practice.

2.2 Potential

A century passed and the world saw great technological advancements in the electronics and computers area. Electric powered devices got efficient to the point that now they no longer need to be connected continuously to a power source, such as a wall socket. They can now work autonomously powered by a small battery. Despite this level of freedom, there is the obvious limitation of the battery autonomy. Companies that produce such devices try to improve their battery without increasing price, weight and safety.

The interest of wireless power transfer was then reborn again in order to solve this challenge [2]. If these equipment could be recharge anywhere without resorting to any additional hardware attached to it, autonomy wouldn't be a problem anymore and, depending on the covered area, batteries could be smaller and these devices could be lighter and safer.

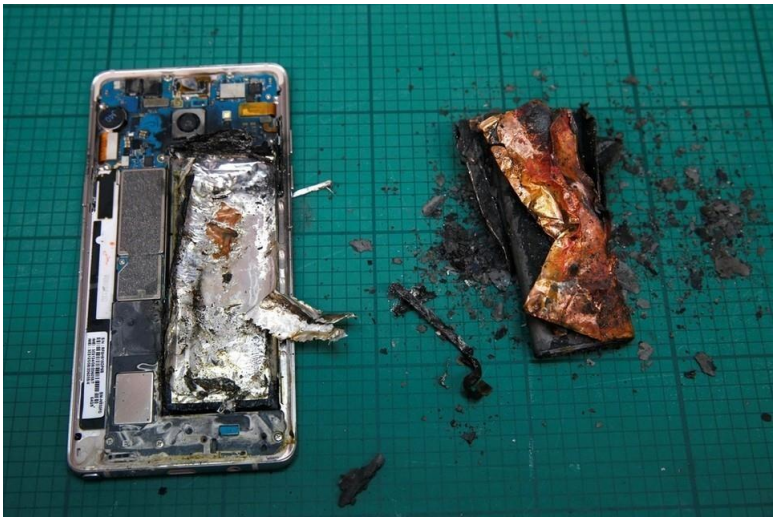

Figure 2.3 - High-end cellphones have high performance and need a bigger battery to last as much as a regular cellphone. If not properly designed, catastrophic failures can happen

In industrial settings, hand-held power tools use mostly battery as power source. For the work be uninterrupted, workshops have multiple equipment or batteries to use for one task. While the worker is using one, the other is recharging and another one for backup. To solve this situation with a bigger battery, the tool would be heavier, making the task more demanding. In addition to solving the type of problem, powering them wirelessly would make these situations easier and more economical.

Figure 2.4 – In factories, most tasks can be performed using only one tool, but the workers need charge them during the shifts, so they need two, in order to make the task interrupted.

Electric cars have gaining popularity over the year. The car companies are starting to offer more models, thus making them a big part of the market. They are safer, cleaner, easier to produce and maintain and perform just as well as conventional cars. Their drawback is the autonomy. Combustion cars can ride for 600 Km, spend around 3 minutes filling the fuel tank and ride another 600 Km. Currently, electric cars cannot make this distance in one charge and takes longer to recharge their batteries to full capacity.

Figure 2.5 - Tesla Model S P100D has the longest distance range with 547 Km in one charge, at in a average speed of 100Km/h and can fast charge in 15-30 minutes

Cars makers are betting in fast charging stations to work around this barrier. Still it takes 5 times longer than refilling a regular gas tank. One possible solution is to charge the batteries while driving on the highway through roads that create an

electromagnetic field that can power cars in movement, without drivers needing to stop their cars to charge them.

In medical applications, implanted devices such as pacemakers run in resort to batteries, which need to be replaced regularly. This requires the patient to be submitted to surgery every time the battery needed replacement. Transferring power wirelessly to these devices would make the procedures unnecessary and would avoid any surgical risk.

2.3 Technology

At the moment, there are three main techniques being studied to transmit power wirelessly, each one having their disadvantages, benefits and operation distances.

2.3.1 Microwaves

Microwaves are used mostly for communication. The applications ranges radios and satellites to GPS (Global Positioning System) and radars. They are also found in microwave oven to heat food by the principle of dielectric heating.

The necessity of humanity to find a new sustainable energy source for earth civilization, gave microwave a new purpose: harvesting solar power from space and sending it back to earth, with great efficiency. The idea was first idealized in 1968 [3], but only after the nuclear disaster in Fukushima, Japan, that the project started being seriously considered. Lacking space for large solar and wind farms, Japan is betting in generating energy from space and transferring through microwaves to a base on earth. This would be possible by creating a geosynchronous SPS (Solar Power Satellite) in orbit at 36.000 Km from the ground, which would gather energy from the sun directly from space. Then, this energy would be converted from DC to microwave, sent to a receiver, converted back to DC, then to AC and power the grid. A scheme of this project can be seen in figure 2.6. This method is more efficient than generating power from regular solar panels on the ground, because microwaves have less attenuation on the atmosphere than solar rays, thus harvesting power from the sun more efficiently, regardless of the time of the year or the weather. To improve its efficiency even more, different types of SPS have been invented, from simple non-concentrators to complex concentrators.

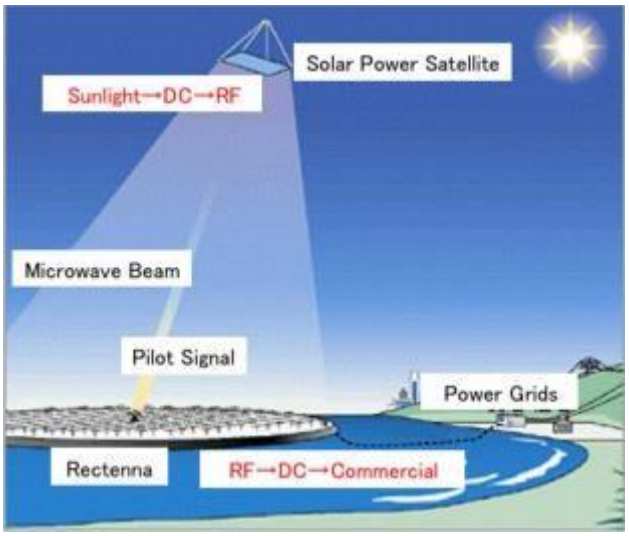

Figure 2.6 - A possible configuration for microwave power transmitter system

The overall system, taking into account the conversion from DC to microwave and vice-versa, the attenuation of the propagation and in the atmosphere, is estimated to have a little less than 50% efficiency, which is more than most modern-day power plants. The DC-microwave is already 70%, as low cost. JAXA (The Japan Aerospace Exploration Agency), the leading organization researching this technology, made a successful experiment in transferring 1.8 KW at a distance of 55m and expect to fully implement a operational plant in the next 30 years.

Similar technic was implemented to power an unmanned plane [4]. UAVs (unmanned aerial vehicle) or drones have their time or operation limited by fuel capacity. Using the same technique from sending power from space to earth, they can, theoretically, fly for unlimited hours, with power being transfer wirelessly, as seen in figure 2.7.

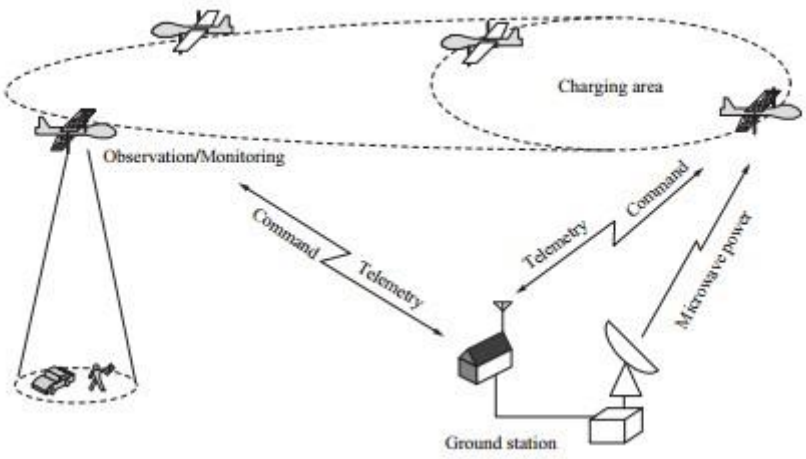

Figure 2.7 - Concept of surveillance UAV, powered by microwaves

Although viable to this purpose (long distance wireless power transmission), using it to power individual electronic devices isn't practical. The transmitter and receiver must have a clear line-of-sight and be perfectly aligned. In order to achieve such perfect alignment, these systems must have complex targeting mechanisms. Although microwaves are not in the ionizing electromagnetic spectrum, it can increase temperature of living organism to dangerous levels. In such application, it is potential dangerous to an unprotected person to be exposed to such a high energizes microwave beam.

2.3.2 Electromagnetic Induction

The principle of electromagnetic induction is vastly used in many areas for different purposes. Electric AC machines and motors, voltage transformers and, of course, the Tesla Coil.

Radio communication uses the same principle and it works because the signal, although travels long distances and suffers losses in the process, requires little power to induce a signal in the receiver. Although, this was the initial idea from Nikola Tesla, with his Wanderclyffe Tower, transmitting power over long distances using electromagnetic wave is highly inefficient. The intensity of the wave generated by the field in the transmitter antenna decreases at square of the distance. However, this application uses signals and antennas sizes designed so that the wave is operating in the far-field, which is perfect for long distances communication. [5]

Our interest lies in the near-field operation, where the antenna´s radius is much smaller than two times the wavelength $(r \ll \lambda)$ and the energy in the magnetic and electric fields have a bigger role in the interactions. Here, power transfer can be done more efficiently. A simple example of its application is an electric toothbrush (figure 2.8). They are designed to be used in bathrooms, where electrocution is a major risk. To avoid expose contacts, an inductor is constructed inside and is excited from another inductor in the base of the toothbrush. Due to the distance between the two, the efficiency of this transfer is huge and, since it is always in contact with the base when not in use, the battery is always charged up and ready for use.

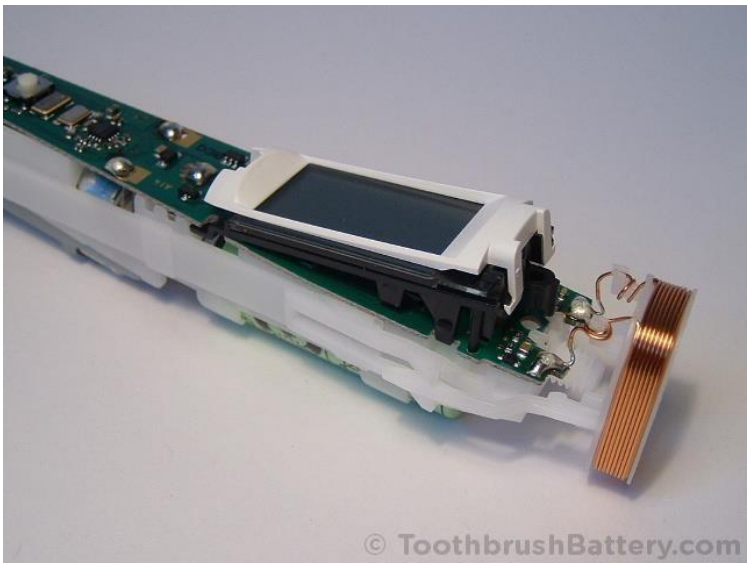

Figure 2.8 - A deconstructed electric toothbrush. The coil on the end charges the batteries through induction without been expose

RFID (Radio frequency identification) is another example of induction in the near-field It explores both power transfer and communication. A source creates an EM field that will interact with a tag, like the one in figure 2.9. These tags consist of an antenna (coil) and an integrated circuit, which will determine the impedance of the tag. Depending of the impedance of the tag, the secondary coil will create a particular response in term of EM reflected wave and both circuits communicate. This interaction results from first coil inducing a current in the second coil. This happens in passive tags. In active tags, there is a source on the tag that will generate the response field. This technology can be found in identification cards, anti-theft systems and as a substitute for bar-codes.

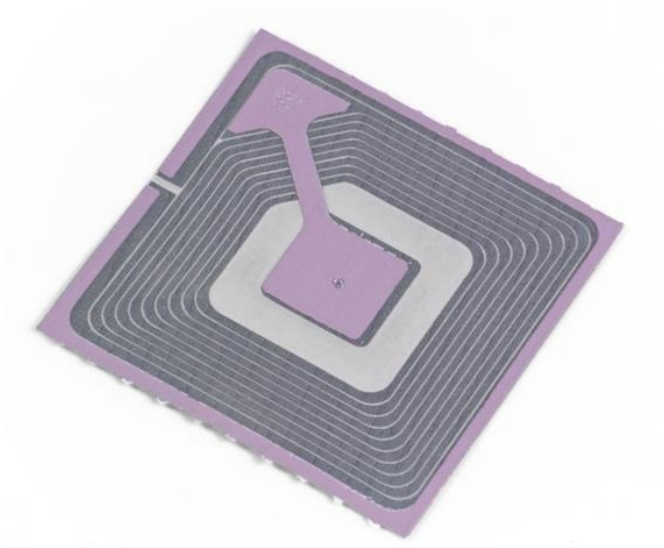

Figure 2.9 - A RFID tag

RFIDs can also operate in the far-field, using the same principle, but is limited to the power required of the tag. On the other hand, working in the near-field limits the distance between the tags [6] (around 10 cm). For transferring power wirelessly using induction, this is exactly the challenge to overcome.

The EM connection between both circuits can be measured with the coupling coefficient k, which is a relation between the coils. Transformers have high efficiency (around 98%), because they can conduct almost all the flux generated from the one of the coils to the other one, through magnetic circuits with high permeability. The problem in loosely coupled circuits is that most of the flux is dissipated in the open space and very little manage to pass through the second coil. A RFID can be represented as in figure 2.10.

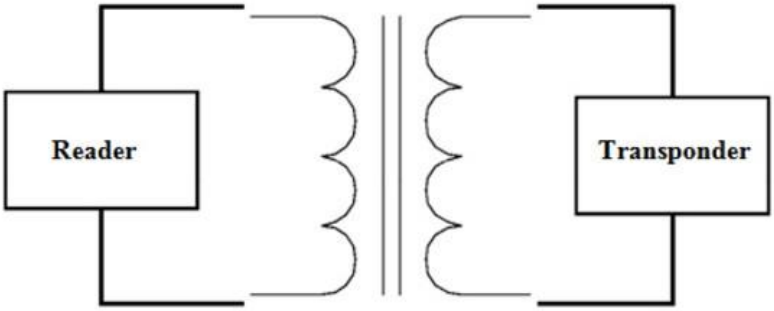

Figure 2.10 - A RFID working in the near-field can be seen as an air-cored transformer

Essentially, many researches try to improve the coupling using resonance between the two circuits [7] [8] [9]. The quote, in the beginning of the chapter, shows how Dr. Tesla already knew the importance of resonance for wireless power transfer. The premise is basic, any resonant system, being it electromagnetic, acoustic or mechanical, have a stronger interaction when working at the same natural frequency, like happened to the Tacoma Narrows Bridge.

Figure 2.11 - the Tacoma Narrows Bridge collapse is one of the best examples of mechanical resonance. The periodic wind blows matched the natural frequency of the bridge's structure. At resonance, the force from the moviments as enough to make it collapse.

In the case of electric circuits, resonance occurs when their impedance are equal in module. However, in coupled circuits the coefficient k influences both circuit, changing the overall resonance circuit and k varies with the distance between the resonators. This means that, for each distance, there is a frequency where maximum power transfer occurs and the circuits have to adjust the impedance to achieve it. The research papers referenced before studies this relation between frequency, magnetic coupling and distance. An example of the results of these studies can be seen in figure 2.12.

$$L_m = \frac{\mu_0}{4\pi} \oint_{C1} \oint_{C2} \frac{dl_1 dl_2}{D} \tag{2.1}$$

$$k = \frac{L_m}{\sqrt{L_1 L_2}} = \frac{f_{even}^2 - f_{odd}^2}{f_{even}^2 + f_{odd}^2} \tag{2.2}$$

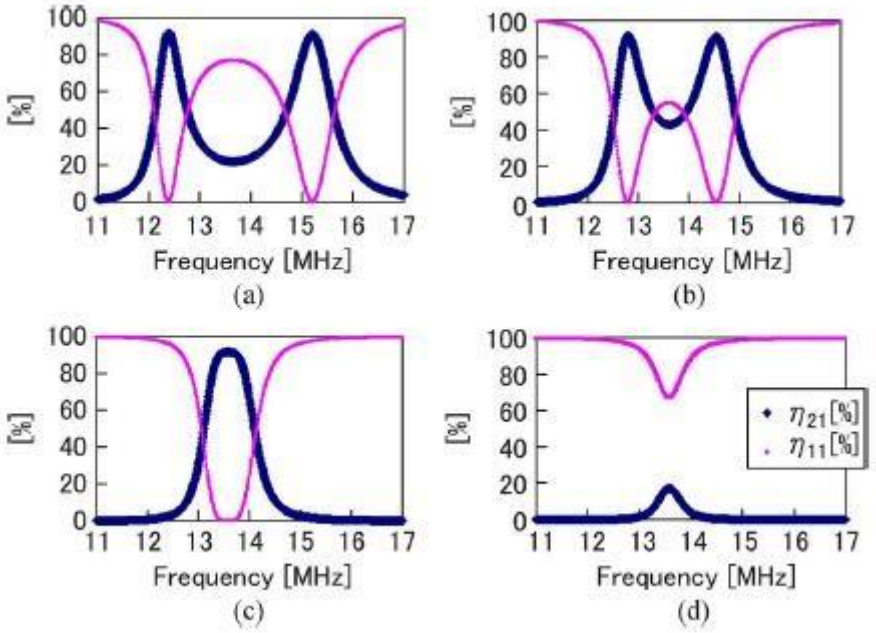

Figure 2.12 – From [7], the blue and pink lines represent the power transfer and reflected, respectively. Each graph illustrates a different gap length: (a) = 49 cm, (b) = 80mm, (c) = 170 mm (d) = 357 mm

Equation 2.1 is the Neumann's formula, which is one of the many ways to calculate the mutual inductance between two circular coils (C_1 and C_2). It is easy to see how the distance affects the mutual inductance. Equation 2.2 shows the relation of coupling coefficient and the inductances at stake in the system. It presents too the split frequencies when is out of resonance from the two circuits.

The technic to adjust the impedance to match to the best frequency for transferring power is using a matching circuit, which is equivalent to adjust a radio knob for better reception. This can be done using many different topologies. Figure 2.13 shows some examples:

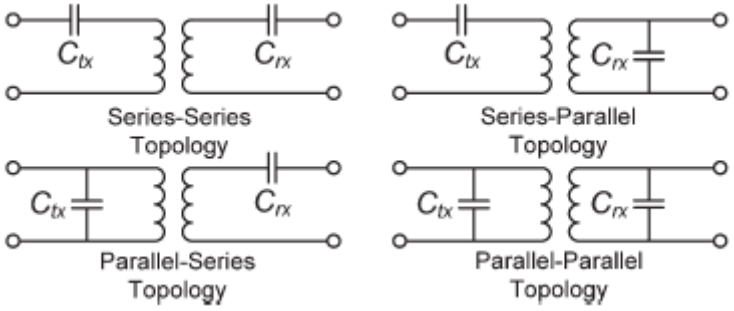

Figure 2.13 - Different matching circuit topologies

Matching circuit can also use inductors in series or parallel to adjust impedance, but they have higher resistive losses than capacitors. Other more complex topologies, mixing series and parallel can be used for better impedance response.

Using resonance to transfer power using induction greatly improve performance when both coil are not in very close proximity. When the impedance and frequency are in the right conditions for a specific k coefficient, efficient power transfer occur. This happens even if the coils are misaligned [11]. This energy in the EM field create to power most electronic devices is not enough to warm humans and animals. MRI uses much powerful field to take images from the body and is considered safe for the international community [12] and the radiation generated at the established frequencies for these applications is non-ionizing. The distance is the biggest limitation of this method. If it is used in application where the coils are not separated more than 30-40 cm, this is a valid method, but if they are further away, the coupling coefficient is minimal, thus minimizing the efficiency, making the system impracticable.

2.3.3 Resonant Coupling + Evanescent Fields

Most authors take the challenge merely as an electric engineering problem and analyze as such. Although possible, the EM coupling is just limited in distances over few centimeters. So instead, a group of researchers from the MIT offered a different perspective, a physic perspective.[7]

They acknowledge the importance of resonance in the process and match their natural frequencies and, in addition of that, they kept in mind the natural losses of regular resonance circuit. Their work focus on the radiation losses, rather than the coupling coefficient, utilizing the phenomenon of Evanescent Fields. This new scheme uses strong coupling. Strong coupling is a regime where a resonator's evanescent waves overlaps with another resonator, thereby achieving the coupling through a method akin to tunneling atop regular resonant induction, and thus strongly reducing transmission loses [7][30]. In other words, the rate of radiation losses is much smaller than the coupling ratio, and this is what defines the strong coupled regime. The experiment can be saw in figure 2.14

This notion of strong coupling is well known in light-matter interactions, but was never tried in this kind of application. Also, in communication applications, the design is the opposite of this, because "long-tailed" evanescent fields causes interference with nearby devices.

A better explanation will be done in the next chapter on how to define this resonant system in the coupled mode theory and the conditions to operate in the strong coupled regime.

This is the method recommended for wireless power transfer. It has all the benefits of the induction technic and can prolong the distance of efficient operation. Besides that, it

can be designed to have the optimum frequency of operation between 1MHz and 50 MHz [15], which are safe and free frequency band. [17] [18]

Figure 2.14 - Experiment from [15] . The coils transferred 60W with a distance of 2 meters

2.4 Power Source and Inverters

Regardless of the method, all of them need an EM field with a given frequency defined by a current varying in time. In other words, they all need a oscillator to work. In the case of microwaves, where frequencies can range from 300 MHz to 300 GHz, it relies on vacuum tubes to generate the magnetic field. In this work, the drive circuit will not operate in such frequencies, thus this method will be set aside.

Most commercial DC-AC power inverters produces square or sinusoidal waveform with the stipulated frequency of the power grid of the country, 50Hz or 60Hz. The most advanced types use a bridge of IGBTs (figure 2.15) to produce such wave. Some studies [19] [20] use this topology to excite their circuits. Their advantage is being capable of work high amounts of power, because of the capacity of the IGBTs. Their control signal is also simple to create and manage. That is why, this solution is mostly used to power wirelessly high powered system, such as an electric's car battery bank [19].

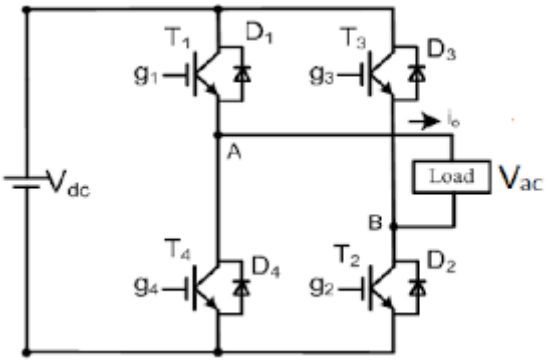

Figure 2.15 – Example of inverter made of a bridge of with IGBTs

In these situations, the area of the created EM field is restricted because of the energy density, that can be dangerous for living beings [17] . The disadvantage is the frequency limitations of the IGBTs. They don't respond well in frequencies above 300 KHz and, in order to transfer high amounts of energy, the frequency is step up instead of the intensity of the magnetic field, for safety reasons. This work aims to have a system where power can be exchanged in an open space, where living beings can circulate, thus this solution is then discarded.

A resonant inverter fits better in this work. They can use components with faster switching properties, allowing the system to operate in higher frequencies. This flexibility is especially important when choosing the operating frequency, because the system will be operating in the high frequency range, which varies from 3MHz to 30MHz, specifically at 13.56MHz. The reason for this particular frequency is because the transmitter creates an EMF strong enough to disrupt others signals using the same frequency, e.g. radio signals. Although there is not a regulated band for wireless power transfer systems, the International Telecommunications Union reserved few frequencies band for uses other than communication, "the Industrial, Scientific and Medical band". The nominal frequency of the system was then chose based on the ISM band [18]. They are efficient and are already use in power purposes, such as inductive heating and fluorescent lighting. [21]

From many RF amplifier topology, the Class-E inverter was chose among the others (e.g. Class-D, Class-F and Class-1/F), because the other are significantly bigger and more complex (Class-F and Class-1/F) or offer less output power with high efficiency (Class-D), although they do nullify the drawbacks of the Class-E [22], the major being the switch stress, due to the high voltage peak. Figure 2.16 shows a Class-D inverter and is possible to see it requires two semiconductors and two different driving circuits to operate then. Class-F inverter, seen in figure 2.17, is a Class-E with a filter between the semiconductor and the resonant tank to manage the harmonics in the output wave and having a better response in the system. This step would make the calculations significant more complicated and wouldn't add much value to this project.

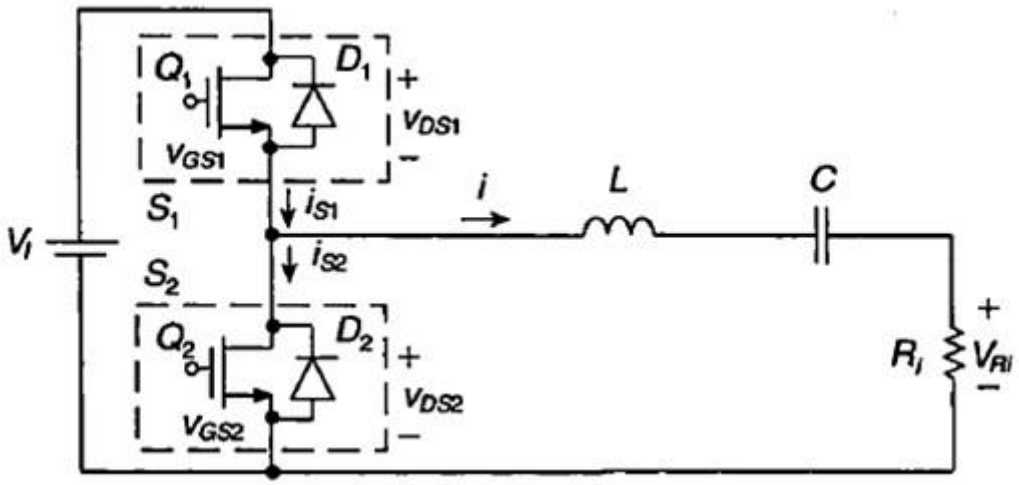

Figure 2.16 – Example of a Class-D inverter

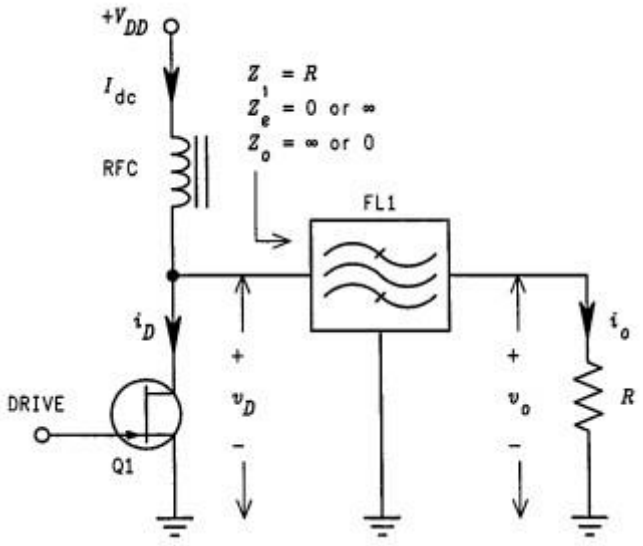

Figure 2.17 - Example of a Class-F inverter

Chapter 3
Coupled Mode Theory and Class-E inverter

This chapter briefly describes the Couple Mode Theory, applies it to define the resonance system between two inductors. Based on that, it establish the proper conditions to the system operate in strong coupled regime. It also provides an explanation on the operation of a Class-E inverter, the design of the driver's antenna and to design and tune the matching circuit. All this sub-circuits together form the driver circuit or excitation circuit, as seen in the figure 3.1.

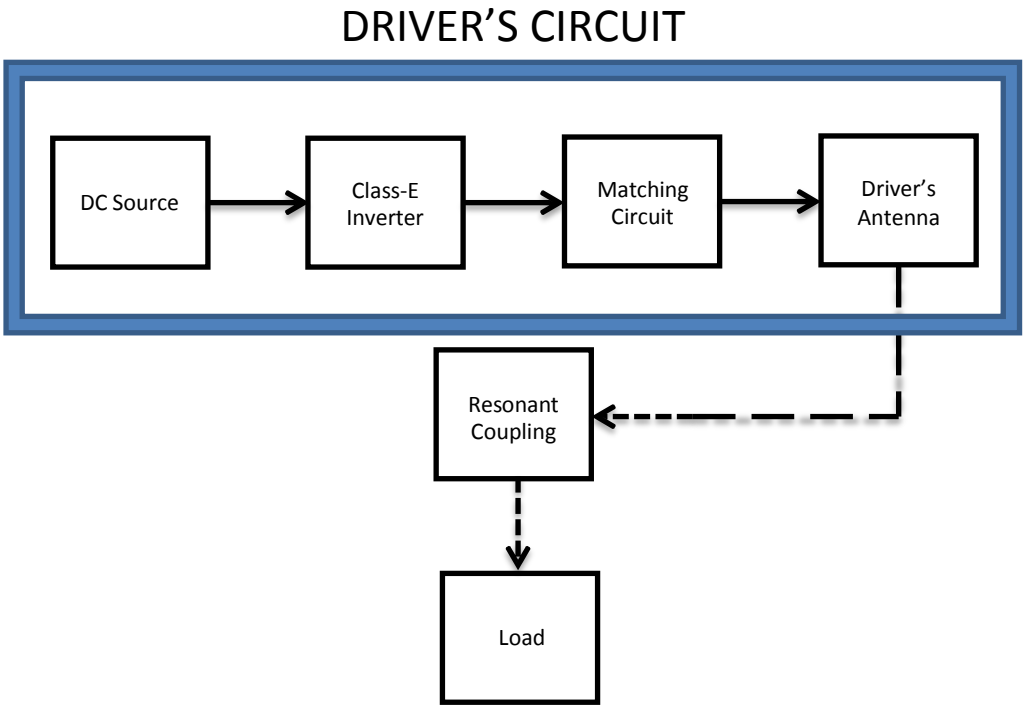

Figure 3.1 - Wireless power transfer system

3.1 Coupled Mode Theory

3.1.1 Introduction – The Coupling of Modes

To analyze the resonant system, the formalism of the CMT will be implemented. The phenomenon of resonance can be seen in many different fields of nature and forms, such as magnetism, acoustic, mechanical etc. Classical examples of resonance are the

spring and mass model and a RLC or a LC circuit. In both cases the basic equation that represents these systems is a second-order differential equation, which is solved rather easily when all parameters values are known. Since most practical projects involves a higher complexity involving external influences, i.e loses, input wave or forces and, especially in the case of this study, a coupling influence from another resonant circuit.

Using this formalism, the system will be represented, taking into account all influences that affect the efficiency and then explore the parameters to achieve resonance between the two resonators and operate in the so called "***Strongly coupled regime***", the region where the efficiency of the power transfer is at its maximum in resonance systems.

The CMT model is valid exactly for this optimal operational regime of well-defined resonances. Its range of applicability does not include very-close-distance coupling, since there the necessary condition $k \ll \omega_{1,2}$ does not hold, neither large-distance far-field coupling, since it fails to predict far-field interference effects and accurate radiation patterns; rather CMT is exactly suitable for the medium-distance near-field coupling of our interest. [14]

This representation can be used to represent any system with similar characteristics.

3.1.2 Formalism

To better understand the terms in the definition, one must understand the definition of a mode and its representation. An electromagnetic mode is an electromagnetic power that exists independent and different from other electromagnetic power. To utilize this definition, a LC circuit, as seen in figure 3.2, is analyze, which will end up been used to define the antennas of the coupled system.

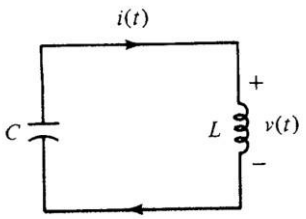

Figure 3.2 – A regular LC Circuit

The basic equations for the LC circuit are:

$$v = L\frac{ai}{dt} \tag{3.1}$$

$$i = -C\frac{av}{dt} \tag{3.2}$$

Where is coil's inductance and C is the capacitor's capacitance. The second-order differential equation of the circuit is given by merging the two equations:

$$\frac{dv^2}{dt^2} + {\omega_o}^2 v = 0 \tag{3.3}$$

Where,

$$\omega_o^2 = \frac{1}{LC} \tag{3.4}$$

Instead of using the first-order differential equation (3.3), two complex variables are defined in (3.5): [23]

$$a_{\pm} = \sqrt{\frac{C}{2}}\left(v \pm j\sqrt{\frac{L}{C}}i\right) \tag{3.5}$$

$a_{\pm}$ is the ***amplitude mode***. To visualize the connection between these equations with the LC circuit, the solution for (3.1) and (3.2) are merged with (3.5):

$$v(t) = |V|\cos(\omega_o t + \varphi) \tag{3.6}$$

$$i(t) = \sqrt{\frac{C}{L}}|V|\sin(\omega_o t + \varphi) \tag{3.7}$$

Where $|V|$ is the amplitude of the voltage in the LC circuit and φ is the phase. Then:

$$a_+(t) = \sqrt{\frac{C}{2}}\left[|V|\cos(\omega_o t + \varphi) + \sqrt{\frac{L}{C}}\left(j\sqrt{\frac{C}{L}}|V|\sin(\omega_o t + \varphi)\right)\right] \tag{3.8}$$

$$= \sqrt{\frac{C}{2}}|V|[\cos(\omega_o t + \varphi) + j\sin(\omega_o t + \varphi)]$$

$$= \sqrt{\frac{C}{2}}Ve^{j\omega_o t}$$

It's possible to calculate the energy in the circuit as:

$$|a_+|^2 = \frac{C}{2}|V|^2 = E \tag{3.9}$$

Where E is the capacitor power, that we will be exchanging with the inductor.

Since a_+ has the dependence $e^{j\omega_o t}$, we can then represent a isolate resonant circuit as:

$$\frac{da_+}{dt} = j\omega_o a_+(t) \tag{3.10}$$

$$\frac{da_-}{dt} = j\omega_o a_-(t) \tag{3.11}$$

Equations (3.10) and (3.11) are ***the positive-frequency component*** and ***the negative-frequency component*** of the mode amplitude. In this case, only the positive component is useful, since it is only the complex conjugate of the positive component [23], reducing the complexity of the system from two differential equations to one. This will especially noticeable when consideration and other parts of the system are added. To simplify the equations appearance, the subscript + is dropped.

The influence from the natural losses of radiated and absorbed radiation of the circuit is represented as a conductance G in parallel with L and C. In the coupled-mode formalism these losses are represented as a ***decay ratio*** $\frac{1}{\tau}$ of the energy stored in the system. This new representation can be seen in figure 3.3 and in equation (3.12):

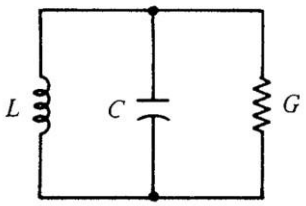

Figure 3.3 – Conductance represents a loss in the LC circuit

$$\frac{da}{dt} = j\omega_o a(t) - \frac{1}{\tau}a(t) \tag{3.12}$$

This kind of loss is minimal, therefore is considered a perturbation and there is no need to change the basic equation to count it. Since the loss decays exponentially as $e^{\frac{2t}{\tau}}$, it is included in the power of the circuit as:

$$\frac{dE}{dt} = -\frac{2}{\tau}E = -P_d \tag{3.13}$$

Which is similar to calculate the average power loss with the decay ratio:

$$P_d = \frac{1}{2}G|V|^2 = \frac{G}{C}|a|^2 \tag{3.14}$$

Taking into account the energy resonating in the circuit and this small loss, it is possible to calculate its ***Quality factor***:

$$\frac{P_d}{\omega_o E} = \frac{\frac{G}{C}|a|^2}{\omega_o|a|^2} = \frac{G}{\omega_o C} = \frac{1}{Q_o} \tag{3.15}$$

Q_o represents a quality factor from a unloaded and unexcited resonator, taking into account only the losses and energy in a simple LC resonator.

Equation (3.12) can already been seen as a non-ideal antenna and used to represent any lossy antenna, in terms of energy. To this equation it will be introduced the effect of an external incident wave, which will be generated by the resonant drive's antenna. This wave is represented by $k_s s$ and it be added to the system equation (3.12) as:

$$\frac{da}{dt} = j\omega_o a(t) - \frac{1}{\tau}a(t) + k_{sm}S_m(t) \tag{3.16}$$

The term k represents the coupling coefficient between driver's antenna and the transmission coil. For this work, $k_s = 1$, meaning that all power from the incident wave from the driver circuit will be collected by the resonant circuit and there is no reflection from the incident wave. In the literature, it is also mentioned a decay ratio concerning the leakage of power from the incident wave, after excitement of the coil. This kind of loss will not be treated as such, but rather considered as the natural loss of the circuit.

At last, it is added to the equation the second circuit, which has its own mode, with its own resonant frequency, losses etc. Since the equation represents the mode of the first circuit, the second circuit will be as an incident magnetic wave with the characteristic of the second circuit mode:

$$\frac{da_1}{dt} = \left(j\omega_1 - \frac{1}{\tau_1}\right) a(t)_1 + k_{12} a(t)_2 \ + S_m(t) \tag{3.17}$$

Notice that now the system has more than one circuit, the modes and its frequencies must distinguish from each other with indexes. The above formalism can be used for the other circuit, as:

$$\frac{da_2}{dt} = \left(j\omega_2 - \frac{1}{\tau_2}\right) a(t)_2 + k_{21} a(t)_1 \tag{3.18}$$

A weak coupling happen when $|k_{12}| \ll \omega_1$ and $|k_{21}| \ll \omega_2$. In that case, the time evolution of the modes won't be influenced, because that component of the equation is much smaller in comparision. however, if ω_1 is close to ω_2, it will affect it, as $e^{j\frac{(\omega_1+\omega_2)}{2}t}$.

The energy conservation laws restricts k_{12} and k_{21}. The time rate of energy exchange (the definition for the coupling coefficient) must vanish, as such:

$$\frac{d}{dt}(|a_1|^2|a_2|^2) = a_1 \frac{a^*{}_1}{dt} + a^*{}_1 \frac{a_1}{dt} + a_2 \frac{a^*{}_2}{dt} + a_2 \frac{a^*{}_2}{dt} \tag{3.19}$$

$$= a_1^* k_{12} a_2 + a_1 k_{12}^* a_2^* + a_2^* k_{21} a_1 + a_2 k_{21}^* a_1^*$$

$$= 0$$

Because the initial amplitudes and phases of a_1 and a_2 can be set arbitrarily, the coupling coefficients must be related by:

$$k_{12} + k_{21}^* = 0 \tag{3.20}$$

$$k_{12} = k_{21}$$

Assuming the dependence $e^{j\omega t}$ and then obtains two homogenous equations from (3.17) and (3.18), without any external perturbation. Solving it for their natural frequencies, the following roots are found:

$$\omega = \frac{\omega_1 + \omega_2}{2} \pm \sqrt{\left(\frac{\omega_1 - \omega_2}{2}\right)^2 + |k_{12}|^2} \equiv \frac{\omega_1 + \omega_2}{2} \pm \Omega_o \tag{3.21}$$

In this solution is important to notice the effect of the coupling coefficient in the frequencies of the system. The coupling splits the two frequencies. When $\omega_1 = \omega_2$,the difference between the two frequencies is $2\Omega_o = 2k_{12}$. Using the solutions as $e^{j\omega t}$ dependence and supposing at $t = 0$, $(0)_1$ and $(0)_2$ is specified , one finds is:

$$a(t)_1 = \left[a(0)_1\left(cos(\Omega_o t) - j\frac{\omega_2 - \omega_1}{2\Omega_o}sin(\Omega_o t)\right) + \frac{k_{12}}{\Omega_o}a(0)_2 sin(\Omega_o t)\right] e^{-i\frac{\omega_1+\omega_2}{2}t} \tag{3.22}$$

$$a(t)_2 = \left[\frac{k_{21}}{\Omega_o}a(0)_1 sin(\Omega_o t) + a(0)_2\left(cos(\Omega_o t) - j\frac{\omega_1 - \omega_2}{2\Omega_o}sin(\Omega_o t)\right)\right] e^{-i\frac{\omega_1+\omega_2}{2}t} \tag{3.23}$$

Below is the graphic representation of the modes in (3.22) and (3.23):

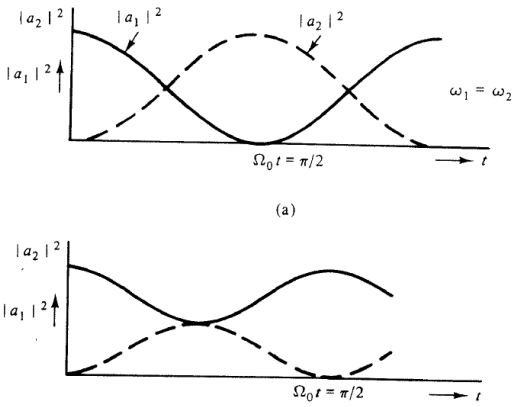

Figure 3.4 – The behaviors of the modes's energy in time

In the first graph, of the figure 3.4, it is possible to notice that in is $t = 0$, a_1 fully excited and at $\Omega_o t = \frac{\pi}{2}$ it is a_2 that is fully excited and so on. The excitation is transfer

from one to another at a frequency of is $\frac{\pi}{k2}$, which is determined by the coupling. In the second graph, which is the general case for the relation between the frequencies of two circuits working without resonance, neither mode is fully excited, meaning that the energy in the modes are not been fully exchanged. This is represented in the efficiency/frequency graph as the ***frequency split***. For a given coupling coefficient, there is a frequency that provides the optimal exchange energy between the resonators. With the variation of the coefficient or the frequencies, the exchange will not be as good as before and that is what it possible to see in the second graph, exchange is still happening but not fully. Some of the energy it is still in one of the resonators. In the case of the second graph, it is in the first one, because the mode energy never reaches the X-Axis.

To complete the system a load is add to it as a perturbation from the second circuit as τ_L. The decay ratio is the power dissipated by it. The whole system is now fully described:

$$\frac{da_1}{dt} = \left(j\omega_1 - \frac{1}{\tau_1}\right)a(t)_1 + k_{12}\left(j\omega_1 - \frac{1}{\tau_2} - \frac{1}{\tau_L}\right)a(t)_2 + S_1(t) \tag{3.24}$$

In a generic form, for n circuits:

$$\dot{a}_m(t) = (j\omega_m - \tau_m)a(t)_m + \sum_{n\neq m} jk_{mn}a(t)_n + S_m(t) \tag{3.25}$$

3.1.3 Efficiency

With all losses of the system established, it is possible to deduce the equation for efficiency using (3.24) to express power for the terms:

$$\eta = \frac{\tau_L\left|a(t)_2{}^2\right|}{\tau_1\left|a(t)_1{}^2\right| + (\tau_1 + \tau_L)\left|a(t)_2{}^2\right|} \tag{3.26}$$

$$= \frac{\frac{\tau_L}{\tau_2}\frac{k^2}{\tau_1\tau_2}}{\left[\left(1 + \frac{\tau_L}{\tau_2}\right)\frac{k^2}{\tau_1\tau_2}\right] + \left[\left(1 + \frac{\tau_L}{\tau_2}\right)^2\right]}$$

Maximum efficiency happens when:

$$\frac{\tau_L}{\tau_2} = \sqrt{1 + \frac{k^2}{\tau_1 \tau_2}} \tag{3.27}$$

The system is highly effective when $k \gg \tau_{1,2}$. This means that the rate of the energy exchange is much higher than the losses ratios from the circuits involved and is represented:

$$\frac{k^2}{\tau_1 \tau_2} \gg 1 \tag{3.28}$$

If the condition given by (3.28) is met, then the system is operating in the ***Strong Coupled Regime***. By standard methods (such as inductive coupling, far-field resonance etc), it is quite difficult to reach this condition. The coupling coefficient decreases at a rate of D^{-3}, when the distance D between the center of the coils is far longer than the characteristic size of the coils. [15] The way proposed in this work is using localized slowly-evanescent field patterns in the near-field to reduce the losses.

3.2 Driver's Circuit

3.2.1 Class-E's Operation and Design Specifications

The basic Class-E circuit is shown in figure 3.5. It consists of a power MOSFET operating as a switch, a L-C-R_i series resonant circuit, a shunt capacitor C_1 and a choke inductance L_f. The MOSFET operates at the frequency determinate by a driver circuit. The shunt capacitor C_1 can be the output parasitic capacitance of the MOSFET, depending of its rating. The L_f inductance is big enough so that the AC ripple of the input current can be neglected. R_i is a resistance representing a AC load. The system is powered by the DC source V_i.

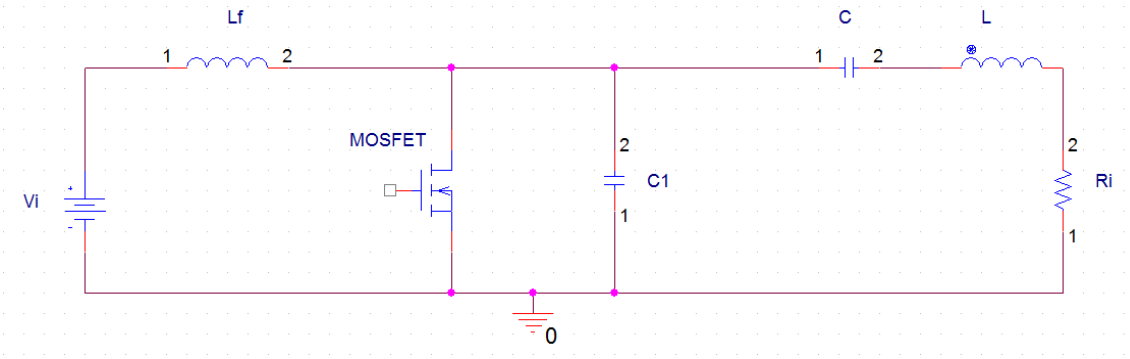

Figure 3.5 - Class-E Inverter topology

The inverter must satisfy two conditions, the voltage across the switch and its derivative dvs/dt are zero when the MOSFET turns on at $\omega t = 2\pi$ to operate in optimum operation. The conditions ensure that the energy storage in $C_1$is not dissipated as heat as turn-on switching loss, because the capacitor and the switch share the same voltage, meaning that when $v_s = 0$, the energy in C_1 is zero. These conditions characterize the inverter as Zero-Voltage-Switching. Figure 3.6 show the voltage across the switch and the current on the load when the inverter is operating in these conditions.

$$\frac{dvs(\omega t)}{d(\omega t)}|_{\omega t=2\pi} = 0 \tag{3.29}$$

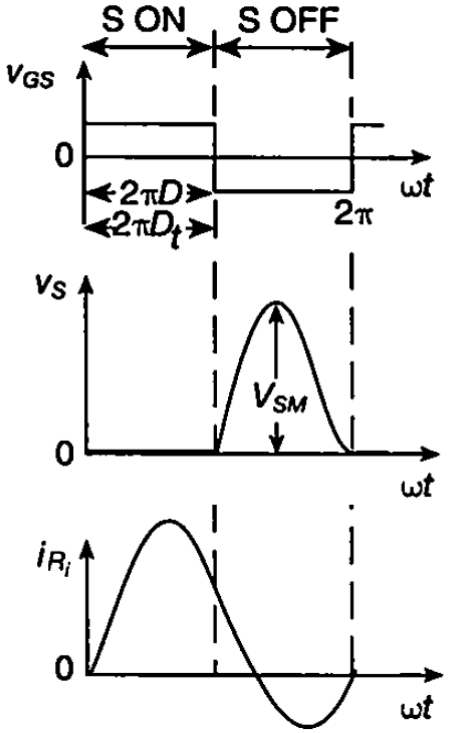

Figure 3.6 - Voltage across switch in optimum operation and current across the load with $Q_L \geq 2.5$

To fulfill these conditions, the operating frequency (f_0) must be between the two resonant frequencies of the circuit. The resonant tank, consisting of L, C, R_i and C_1 will determine the resonant frequency of the circuit, depending on the state of the MOSFET. When the switch is on, C_1 is short-circuited and the circuit becomes a regular RLC resonant circuit with the resonant frequency being:

$$f_{01} = \frac{1}{2\pi\sqrt{LC}} \tag{3.30}$$

When the switch if off, C_1 is in series with C:

$$C_{eq} = \frac{1}{C} + \frac{1}{C_1} = \frac{CC_1}{C + C_1} \tag{3.31}$$

Making the second resonant frequency being:

$$f_{02} = \frac{1}{2\pi\sqrt{LC_{eq}}} = \frac{1}{2\pi\sqrt{L\frac{CC_1}{C + C_1}}} \tag{3.32}$$

The high impedance of the components in the resonant tank also protects the choke inductance against short circuits in the load, preventing them appearing in the switch.

The quality factor Q_L will determine the shape of the current across R_i. To achieve a sinusoidal waveform, $Q_L \geq 2.5$ [10]. With $Q_L < 2.5$, the current will have an exponential waveform. However, a high value of Q_L increases the RMS value of the current across the switch, resulting in greater conducting losses and passive components parasitic losses. In a trade-off between efficiency and the spectral purity, the quality factor must be $Q_L \approx 5$ and it is determined by:

$$Q_L = \frac{2\pi f_0 L}{R_i} \tag{3.33}$$

The voltage source must be chosen based on the MOSFET. The voltage peak across the switch in the Class-E inverter is about 3.6 times the DC voltage when the duty cycle is 50% [24], whence the rated voltage of the device must be picked accordingly. As noted further, MOSFET with high rated voltage also have high output paradisiac capacitance, which can exceed the value of $_1$, making the device unfit for the circuit. For that reason, using high values for the voltage input might limit the choices, depending of the MOSFETs availability. This is one of the drawbacks of this topology. The other one is load sensitivity, which is discussed in the next subchapter.

3.2.1.1 Components Values

The equations for the values of the passive components and the optimum load were taken from [10] and they were obtained through analyzing the topology of circuit and its behavior, considering the following considerations:

1. The MOSFET is considered an ideal switch whose on-resistance is null, off-resistance is infinite and the switching times are zero.
2. The choke inductance is high enough so that the AC component is considered null.
3. The loaded quality factor Q_L is high enough, so that the current through the load is sinusoidal.
4. The duty cycle is 50%.

Figure 3.7 shows all the components and parameters involved in the calculations of a standard Class-E inverter, like the one in Figure 3.6.

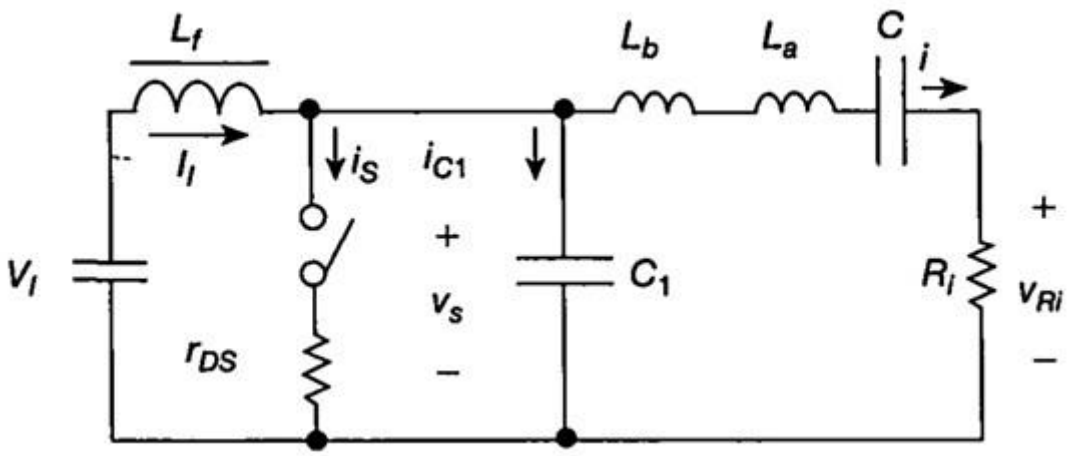

Figure 3.7 – Equivalent circuit of Class-E Inverter working between the two resonance frequencies and its parameters

3.2.1.1.1 Value of Load R_i for Optimum Operation

Analyzing the currents of Figure 3.7 and the taking the 4th assumption:

$$i_s + i_{c1} = I_I - i \tag{3.34}$$

$$i_s + i_{c1} = I_I - I_m \sin(\omega t + \phi)$$

Assuming the D is the driver signal duty cycle, the switch is on in $0 < \omega t \leq 2\pi D$, which implies that $i_{C1} = 0$:

$$i_s = \begin{cases} I_I - I_m \sin(\omega t + \phi), & 0 < \omega t \leq 2\pi D \\ 0, & 2\pi D < \omega t \leq 2\pi \end{cases} \tag{3.35}$$

In the rest of the period, $2\pi D < \omega t \leq 2\pi$, the switch is off, therefore $i_s = 0$:

$$i_{C1} = \begin{cases} 0, & 0 < \omega t \leq 2\pi D \\ I_I - I_m \sin(\omega t + \phi), & 2\pi D < \omega t \leq 2\pi \end{cases} \tag{3.36}$$

Utilizing the equation for the voltage across the shunt capacitor and (3.36) when the switch is off:

$$v_s = \frac{1}{\omega C_1} \int_{2\pi D}^{2\pi} i_{C_1} \, d\omega t$$

$$v_s = \frac{1}{\omega C_1} \left[I_I(\omega t - 2\pi D) + I_m[\cos(\omega t + \phi) - \cos(2\pi D + \phi)] \right] \tag{3.37}$$

It is possible to find the relation between between I_m and I_i, considering the condition $v_s(2\pi) = 0$:

$$I_m = I_I \frac{2\pi(1-D)}{\cos(2\pi D + \phi) - \cos(\phi)} \tag{3.38}$$

By using (3.37) in (3.38):

$$v_s = \frac{I_I}{\omega C_1}\left[\omega t - 2\pi D + \frac{2\pi(1-D)[\cos(\omega t + \phi) - \cos(2\pi D + \phi)]}{\cos(2\pi D + \phi) - \cos(\phi)}\right] \tag{3.39}$$

Since $dv_s/d_t = 0$ at $\omega t = 2\pi$, it is possible to find the angle ϕ in function of D:

$$\tan\phi = \frac{\cos(2\pi D) - 1}{2\pi(1 - D) + \sin(2\pi D)} \tag{3.40}$$

The components L_a and C in Figure 3.7 are in resonance frequency f_{01}, but the working frequency f_0 is above it, therefore the resonant tank is represented by a inductive load composed of L_b and R_i as seen in figure 3.8. Analyzing the circuit:

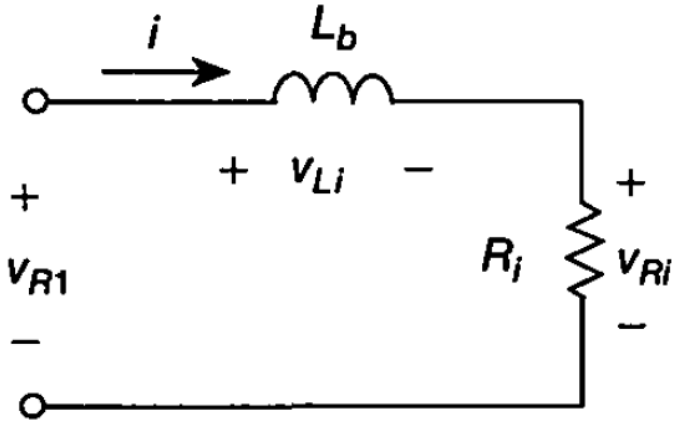

Figure3.8 - Equivalent circuit of the resonant tank working above resonance

$$v_{R_1} = v_{L_i} + v_{R_i}$$

$$= V_{L_{im}} \cos(\omega t + \phi) + V_{r_{im}} \sin(\omega t + \phi)$$

$$v_{R_1} = V_{R_{m1}} \sin(\omega t + \psi + \phi) \tag{3.41}$$

Figure 3.9 is the representation of the voltages and its phases, involved in the in the resonant tank.

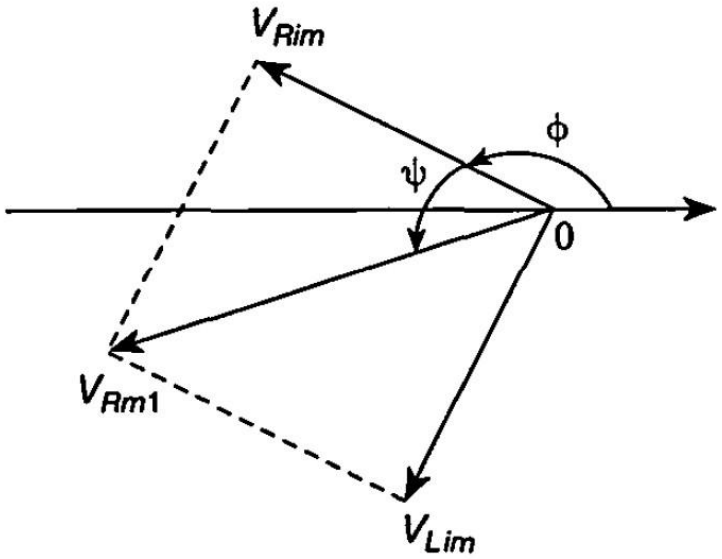

Figure 3.9 - Phasor diagram of the resonant tank at frequency f_0

Using trigonometry techniques in figure 3.9:

$$\tan(\psi) = \frac{V_{L_{bm}}}{V_{R_{im}}} \tag{3.42}$$

The 3th assumption states that the load current is sinusoidal, therefore the higher harmonics are zero. In (3.41), $v_{R_{m1}}$ is the amplitude of the fundamental component of switch voltage v_s. Using (3.39) and the Fourier series formula, the amplitude of the voltage across the load is obtained as:

$$v_{R_m} = \frac{1}{\pi}\int_{2\pi D}^{2\pi} v_s \sin(\omega t + \phi)\, d(\omega t) = -\frac{2\sin(\pi D)\sin(\pi D + \phi)}{\pi(1-D)} V_I \tag{3.43}$$

Combining the definition of power in R_i and (3.43), it possible to calculate the load value for operating in optimum condition using the input voltage and the desire output power chosen:

$$P_{Ri} = \frac{V_{R_m}^2}{2R_i} = \frac{2\sin^2(\pi D)\sin^2(\pi D + \phi)V_I^2}{\pi^2(1-D)^2 R_i} \tag{3.44}$$

Simplifying for D=0.5:

$$R_i = \frac{8}{(\pi^2+4)}\frac{V_I^2}{P_{Ri}} \tag{3.45}$$

3.2.1.1.2 Value of Shunt Capacitor C_1

To calculate the value of C_1 that satisfies the conditions and assumptions, it is necessary to find the relations between the input voltage V_I and current I_I. For this, the input DC resistance of the system is calculated:

$$R_{DC} = \frac{V_I}{I_I} \tag{3.46}$$

To establish the relation, V_I is found as:

$$V_I = \frac{1}{2\pi}\int_{2\pi D}^{2\pi} v_s \, d(\omega t) = \frac{I_I}{\omega C_1}\left[\frac{(1-D)[\pi(1-D)\cos(\pi D)+\sin(\pi D)]}{\tan(\pi D+\phi)\sin(\pi D)}\right] \tag{3.47}$$

Rearranging (3.47) simplifying for D=0.5 :

$$R_{DC} = \frac{V_I}{I_I} = \frac{1}{\pi\omega C_1} \tag{3.48}$$

Substituting (3.48) in (3.47) after simplifying to D=0.5:

$$V_{RI_m} = R_i I_m = \frac{4}{\sqrt{\pi^2+4}}\frac{1}{\pi\omega C_1} I_I$$

$$R_i \frac{I_m}{I_I} = \frac{4}{\sqrt{\pi^2+4}}\frac{1}{\pi\omega C_1}$$

Using the relation of (3.38) with D=0.5:

$$R_i \frac{\sqrt{\pi^2+4}}{2} = \frac{4}{\sqrt{\pi^2+4}}\frac{1}{\pi\omega C_1}$$

$$C_1 = \frac{8}{\pi\omega R_i(\pi^2+4)} \tag{3.49}$$

3.2.1.1.3 Value of Inductance L

The total inductance L is calculated using the definition of the quality factor (3.33) in a series resonant circuit at the working frequency:

$$L = \frac{Q_L R_i}{\omega} \tag{3.50}$$

3.2.1.1.4 Value of Capacitance C

The resonant tank is at total resonance at frequency f_{01}, when the inductance is represented by L_a, but since the working frequency is higher than the resonant frequency, C resonates partially with L, therefor the reactance relation is given by:

$$\frac{1}{\omega C} = \omega L_a = \omega(L - L_b) = Q_L R_i - \omega L_b \tag{3.51}$$

The ωL_b can be calculated the same way as C_1 in (3.47):

$$V_{L_{bm}} = v_{L_i} = \omega L_b I_m = \frac{1}{\pi}\int_{2\pi D}^{2\pi} v_s \sin(\omega t + \phi)\, d(\omega t)$$

Integrating and substituting D=0.5:

$$v_{L_i} = I_m \omega L_b = \frac{\pi(\pi^2 - 4)}{4\sqrt{\pi^2 + 4}} V_I \tag{3.52}$$

Substituting (3.48) in (3.47) after simplifying to D=0.5:

$$I_m \omega L_b = \frac{\pi(\pi^2 - 4)}{4\sqrt{\pi^2 + 4}} \frac{1}{\pi \omega C_1} I_I$$

$$\omega L_b \frac{\sqrt{\pi^2 + 4}}{2} = \frac{\pi(\pi^2 - 4)}{4\sqrt{\pi^2 + 4}} \frac{1}{\pi \omega C_1}$$

$$L_b = \frac{\pi^2 - 4}{2(\pi^2 + 4)} \frac{1}{\omega^2 C_1} \tag{3.53}$$

Using (3.49) in (3.53) :

$$L_b = \frac{\pi^2 - 4}{2(\pi^2 + 4)} \frac{\pi(\pi^2 + 4)R_i}{8\omega}$$

$$\frac{\omega L_b}{R_i} = \frac{\pi(\pi^2 - 4)}{16} = \tan(\psi) \tag{3.54}$$

If one rearrange (3.51), it is possible to directly use(3.54) and find the value for C:

$$\frac{1}{\omega C R_i} = Q_L - \frac{\omega L_b}{R_i} = Q_L - \frac{\pi(\pi^2 - 4)}{16}$$

$$C = \frac{1}{\omega R_i \left[Q_L - \frac{\pi(\pi^2 - 4)}{16} \right]} \tag{3.55}$$

3.2.1.1.5 Value of Choke Inductance L_f

The minimum value for the choke inductance $L_{f_{min}}$ that ensures the peak-to-peak current ripple to be less than 10% of the DC current is given by:

$$L_{f_{min}} = 2\left(\frac{\pi^2}{4} + 1\right)\frac{R_i}{f} \tag{3.56}$$

3.2.1.2 Resume of the components values equations with D=0.5

To calculate the components, the value of the Input voltage , the working frequency f and the maximum power P_{Ri} delivered to the load must be chosen. The equations were calculated and the assumptions and optimum operation were taken into account as described at 2.1.3 e 2.1.2, respectively.

$$R_i = \frac{8}{\pi^2 + 4} \frac{{V_I}^2}{P_{Ri}} \tag{3.45}$$

$$C_1 = \frac{8}{\pi\omega R_i(\pi^2 + 4)} \tag{3.49}$$

$$L = \frac{Q_L R_i}{\omega} \tag{3.50}$$

$$C = \frac{1}{\omega\left[Q_L - \frac{\pi(\pi^2 - 4)}{16}\right]} \tag{3.55}$$

$$L_{f\,min} = 2\left(\frac{\pi^2}{4} + 1\right)\frac{R_i}{f} \tag{3.56}$$

Analyzing the equations, it is possible to notice that all the values are dependable from the load, which makes the ZVS of the Class-E inverter highly sensitive to load impedance. The inverter works in the suboptimum operation when the load is different from the value calculate for R_i in (3.45), reducing the efficiency of the system. If the load is known, it is possible to adapt it by using matching network configurations. The load sensitivity is the main drawback of this topology.

3.2.2 Matching Circuit

3.2.2.1 Introduction

Matching circuits are widely used in telecommunications purposes to match the impedance of source with the load, thus achieving maximum power transfer. Another use for matching circuits is to minimize the reflection coefficient between a receiver and a transmitter. In the case of this work, changing the impedance of the circuit as seen from the inverter (driver's and loop antenna) is necessary to achieve the ZVS, because that impedance does not have the same value or characteristic as the load used to design the inverter. In figure 3.10 is possible to see how the Drain-Source voltage on the MOSFET is affected by a mismatch of the load impedance.

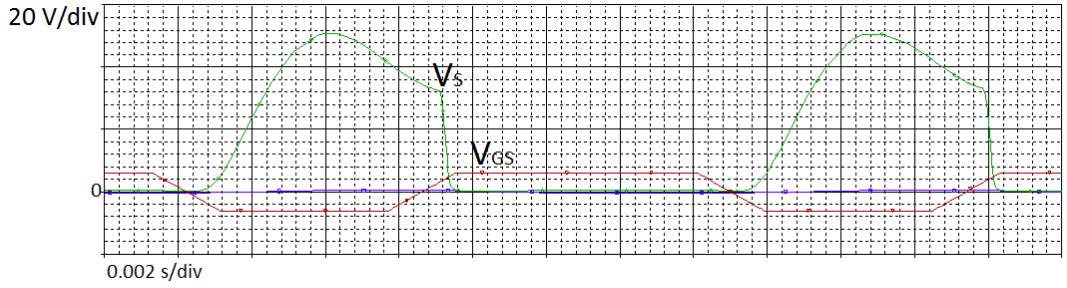

Figure 3.10 - Drain-Source voltage waveform with load mismatch ($R_I = 50\Omega$)

Depending of the load and transmission line characteristics, the matching circuit can have different topologies. On this work, the topology used is two capacitors in "L", so that the real and the imaginary part of the load impedance can be transformed. Using one capacitor in parallel is enough for transforming both parts of the impedance, but adding the second capacitor in series makes it simpler to tune after the calculations. It's also possible to use a inductor in series instead of the capacitor, but the capacitor is much more efficient than a normal inductor and easier to adjust to the desirable value. [8]

The steps from [25] will be used to the make the calculations. This application note is a guide to design an antenna, a matching circuit and EMC filter for a RFID application. The EMC won't be necessary for this application.

3.2.3 Driver's Antenna

3.2.3.1 Setting up the Antenna

An antenna can be represented as RLC circuit, as seen in figure 3.11:

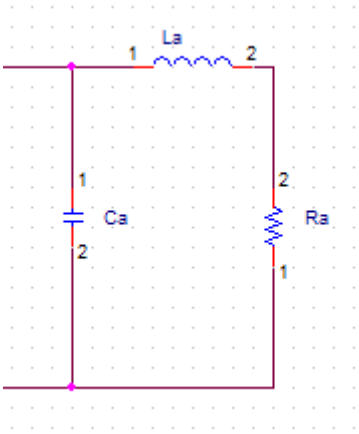

Figure 3.11 – Antenna's Equivalent Circuit

The antenna design will determine its inductance. All parameters will have an influence on the value: shape, radius, number of turns, coil diameter and space between the turns. In the next sub-chapter an explanation will be displayed about how these parameters will play out in the design of the antenna. At this stage, the antenna will be set-up to connect to the matching circuit.

The equivalent circuit of the antenna consists of an inductance, a capacitance and a resistance. The inductance represents the antenna's self-inductance and later the combination with the mutual inductance between the receiver and the transmitter coils. The capacitance is the parasitic capacitance created between the turns of the coil. This

component and the inductance will determine the self-resonance frequency of the antenna by the formula:

$$f_{a1} = \frac{1}{2\pi\sqrt{C_{1a}L_{a1}}} \tag{3.58}$$

After designing the Antenna, it's necessary to make sure that $f_{a1} \geq 35\ MHz$ by keeping the capacitance as low as possible. If the design fails to meet this requirement, the antenna will be seen by the circuit as a short-cut (if $f_{a1} = 13.57\ MHz$, the same frequency as the system) or as a capacitance, resulting in most of the current conducting through the capacitor, therefor not creating the necessary magnetic field to induct the receiver coil. The resistance is the natural resistance of the coil and will determine the quality factor of the antenna:

$$Q_{a1} = \frac{\omega L_{a1}}{R_{a1}} \tag{3.59}$$

Ideally $Q_{a1} \cong 30$, because that value will grant a wider frequency band for the antenna. Since the antenna will be made of copper wire, the resistance will be too low for the quality factor to be close to 30. So an additional resistance R_{Q1} will be added in each terminal of the antenna, with the value of:

$$R_{Q1} = 0.5\left(\frac{\omega L_{a1}}{30} - R_{a1}\right) \tag{3.60}$$

The new configuration is seen in Figure 3.12:

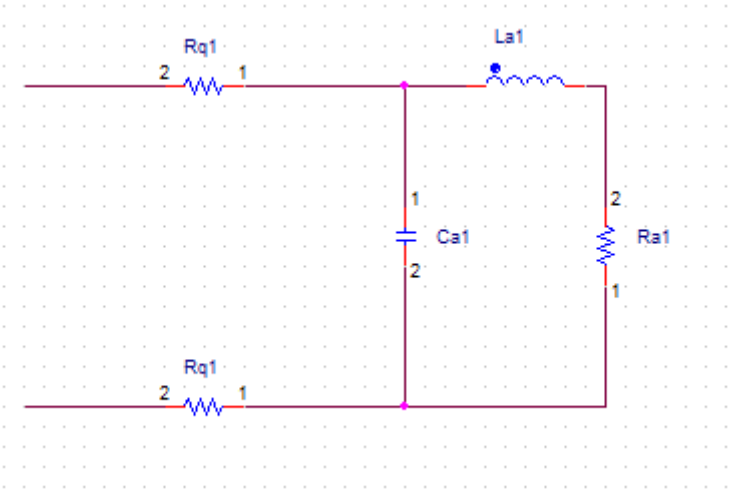

Figure 3.12 – Transmitter Antenna with Damping Resistors in each terminal

3.2.3.2 – Components Calculations

For next step, it is necessary to calculate the parallel equivalent circuit of Figure 3.12, because of the approximations considered in the equations. The parallel model is seen in figure 3.13:

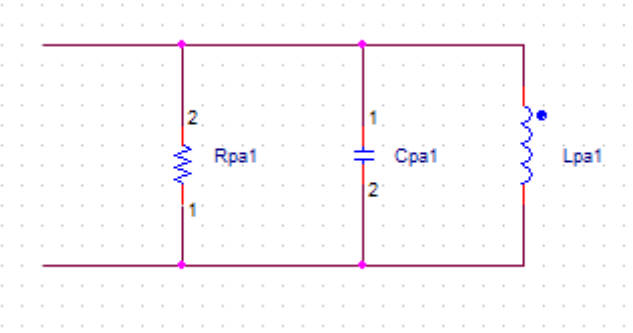

Figure 3.13 – Transmitter Antenna Parallel Equivalent Circuit

With the new values being:

$$L_{a1} \cong L_{pa1}$$

$$C_{a1} \cong C_{pa1}$$

$$R_{pa1} \cong \frac{(\omega L_{a1})^2}{R_a + 2R_{Q1}} \tag{3.61}$$

The equations for the values of the serie and the parallel capacitors are:

$$C_2 \approx \frac{1}{\omega\left(\sqrt{\frac{R_{tr}R_{pa}}{4}} + \frac{X_{tr}}{2}\right)} \tag{3.62}$$

$$C_3 \approx \frac{1}{\omega^2 \frac{L_{pa}}{2}} - \frac{1}{\omega\sqrt{\frac{R_{tr}R_{pa}}{4}}} - 2C_{pa} \tag{3.63}$$

Where R_{tr} and X_{tr} is the target of the impedance transformation, thus:

$$R_{tr} = R_i$$

$$X_{tr} = \omega L - \frac{1}{\omega C}$$

Figure 3.14 shows the representation of the antenna and the matching circuit. If correctly designed, this circuit is seen as a single resistance from the inverter.

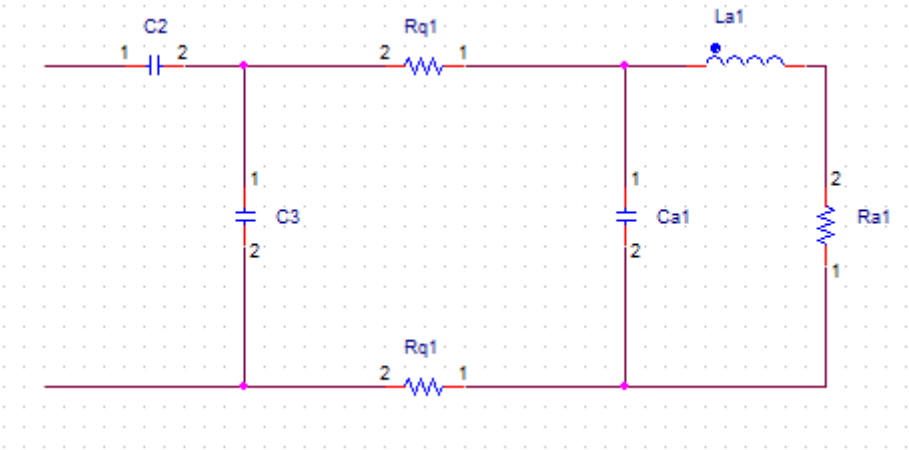

Figure 3.14 - Transmitter Antenna with Damping Resistors and Matching Circuit

3.2.3.3 Antenna's Inductance Calculation

The inductance value is directly affected by the size and shape of the coil, as described by Faraday's law. The desirable size for the driver's antenna relies on the scale of the overall system, more specifically the transmitting coil, because, to maximize the coupling between both coils, they must be concentrically and axially aligned. For the shape, an Archimedean antenna was chosen because it offers better size/inductance ratio.

For simulation purpose, an inductance value must be considered and will be calculated using the method described in [1]. The sum of all potential vector generated by the magnetic field along the coil will be calculated using matlab:

$$\vec{A} = \frac{\mu_0}{4\pi}\left[\int \frac{I}{D} dx\vec{e}_x + \int \frac{I}{D} dy\vec{e}_y + \int \frac{I}{D} dz\vec{e}_z\right] \tag{3.64}$$

The Archimedean shape is represented in the three axes as:

$$x = r\cos\theta$$
$$y = r\cos\theta$$
$$z = z$$

I is the current and *D* is the distance between the two points of the potential vector and this differential length and is determined by the position of the "sensing coil", which is a mirror coil that senses the drive's coil. To calculate the self-inductance, it is desirable

that both coils are in the same position to minimize D, thus giving a more precise inductance value. In the simulation, they cannot be overlap, otherwise $\vec{A} = \infty$. Therefore they have a slight adjustment in the z axis. The calculations ware made using 1000 steps along the coil, but more could be used for more precise values, at cost of computational processing power. The self-inductance is then calculated as:

$$L = \frac{1}{I}\int \vec{A} \cdot \overrightarrow{dl} = \frac{1}{I}\left[\int dx\vec{e}_x + \int dy\vec{e}_y + \int dz\vec{e}_z\right]$$

To graphically represent the antenna and simpler relation with the design values, a general view using polar coordinates, considering the number of turns (N) and inner (R_m) and outer (R_M) radius, can be written as:

$$r = R_m exp\left\{\frac{\theta}{2\pi N} ln\left(\frac{R_M}{R_m}\right)\right\} \tag{3.65}$$

Where is the distance from the center of the antenna. The inner radius is affected by the conductor radius (T_s), the number (N) and spacing between turn (T_s) as:

$$R_m = R_M - (NC_D + (N-1)T_s) \tag{3.66}$$

Chapter 4
Simulations, Tuning and Results

4.1 Simulation parameters

4.1.1 Components calculations and choice

To verify the components value, the inverter was simulated using OrCAD PSpice. The inicial parameters are:

V_i	80 V
P_i	200 W
f	13.57 MHz
Q_L	5
D	0.5

The inverter components were calculated using the equations from the previous chapter 2.1.3.6:

R_i	18.5 Ω
L	1.08 µH
C	165 pF
C_1	116 pF
L_f	12 µH

The right selection of the semiconductor is of major importance. Since the characteristics of the MOSFET are tightly related (like the Drain-Source voltage and the output capacitance), it may be difficult to find a component that has the specification compatible with the system design, as explained below.

The first consideration the designer must have is that the MOSFET can operate efficiently at the desired frequency. The next condition is the rated Drain-Source voltage, which must be higher than V_{SM} voltage (seen in Figure 3.6), which is given by the equation [24]:

$$V_{SM} = 3{,}562 * V_I \tag{4.1}$$

Comparing equation (4.1) with (3.45), it is possible to conclude that to achieve a considerable amount of power delivered to the load, with a reasonable load resistance

value, the rated voltage of the MOSFET must be relatively high, which leads to a problem concerning the output capacitance. Most of the semiconductors that have high Drain-Source voltage have high values of output capacitance and that can be incompatible with the value calculated in (3.49). It is desirable that the value be higher than the one in the datasheet, because this value can be later achieved with a parallel capacitor. Since the output capacitance varies with the Drain-Source voltage in a highly nonlinear manner, it makes it difficult the predict the exact value of the parasitic capacitance, so it is recommendable to have a variable capacitor for C_1. The design must have a balance between input voltage and output power that demands a realistic MOSFET and also keeping in mind the requirements of the overall system.

Based on the previous considerations and the results of the equations, the model SIHP8N50D from Vishay® was selected for simulation because it fits all the requirements for a proper operation. The model used in PSpice was provided from the manufacturer, so it is assumed that the model is accurate enough.

4.2 Class-E simulation Results

With the components calculated, it is possible to simulate the circuit. In figure 4.1, C_1 is already compensating the output capacitance of the MOSFET.

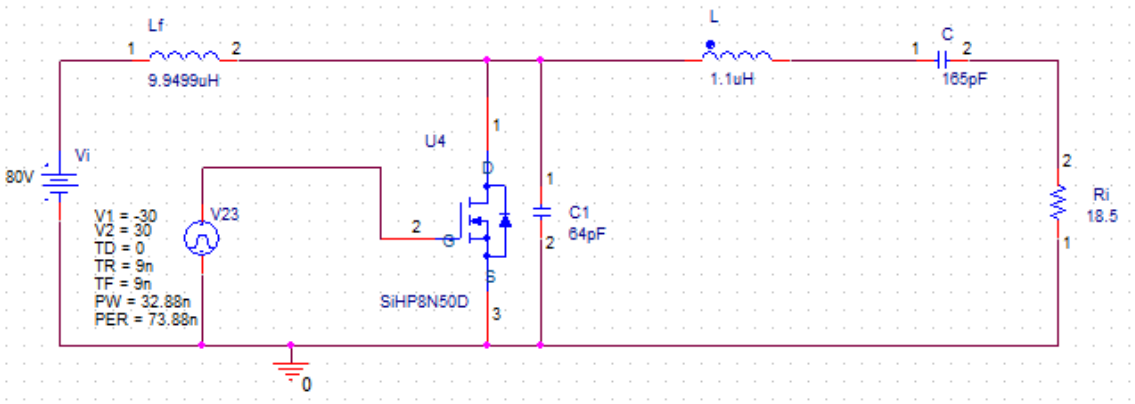

Figure 4.1 – Designed Class-E Inverter

The gate signal is generated by a pulse source working with 50% duty cycle and voltage necessary to conduct the MOSFET, according with the datasheet. Figure 4.2 shows the expected voltage waveform (as seen in Figure 3.6), but the Zero-Voltage Switching condition is not satisfied, which means that the circuit is well designed but is not tuned.

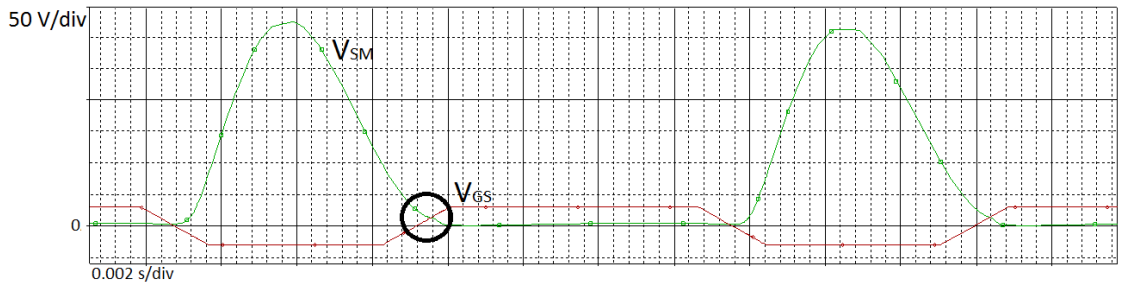

Figure 4.2 – Drain-Source voltage waveform without tuning C_1

That is the consequence of the MOSFET's non-linear output capacitance. C_1 value was swept between 1pF and 100pF and the voltage was graphically analyzed. Tuning C_1 too low will make the voltage lower to zero too soon, decreasing the output power, and will increase the peak voltage significantly, putting in danger the semiconductor (Figure 4.3). Tuning C_1 too high will have the opposite effect (Figure 4.4). Depending of the purpose of the inverter, C_1 can be increased, without changing the value of other components, to deliver more power at the cost of efficiency, but the aim of this work is to achieve power transfer with highest efficiency possible.

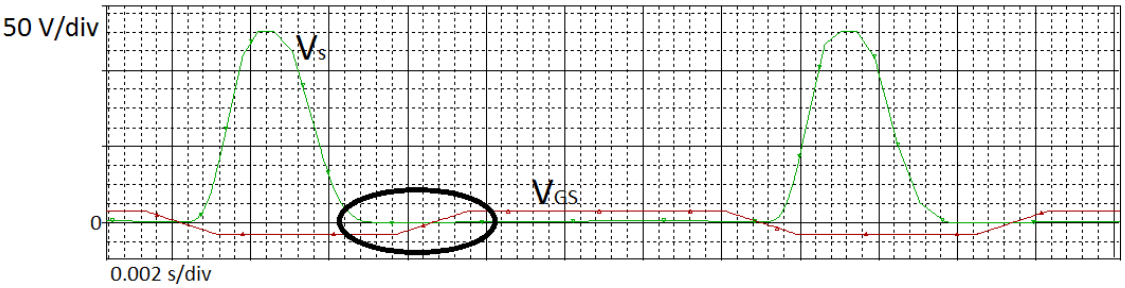

Figure 4.3 – Drain-Source Voltage with $C_1 = 1pF$

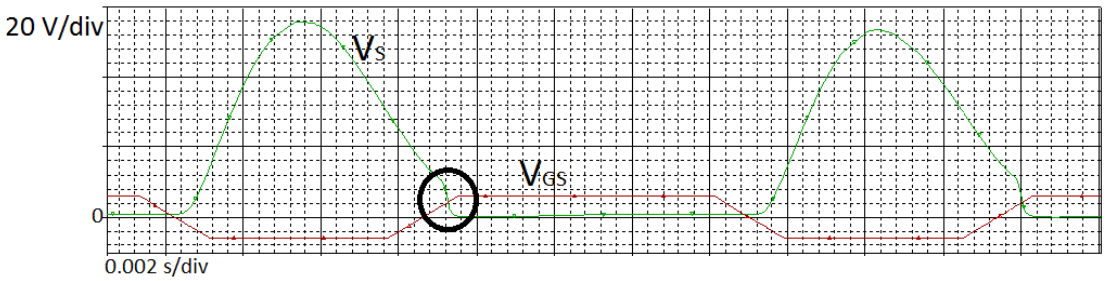

Figure 4.4 – Drain-Source Voltage with $C_1 = 100pF$

The balance between output power and efficiency was obtain with the parallel capacitance $C_1 = 45pF$. Since the drain voltage is higher than the one state for the

output capacitance on the datasheet, it is expected that the value for the output capacitance in the simulation to be higher. Therefore the ideal value for the parallel capacitance is lower than the one calculated. In Figure 4.5 it is possible to observe that the voltage is close to zero when the MOSFET starts to conduct ($v_{GS} \approx 30$), reducing to practically zero the switching losses. Ideally, under these conditions, the only loss would the conduction loss, given by the drain-to-source resistance. Although the Drain-Source voltage increased, it is still 66% of the semiconductor's rated voltage, making it safe to use.

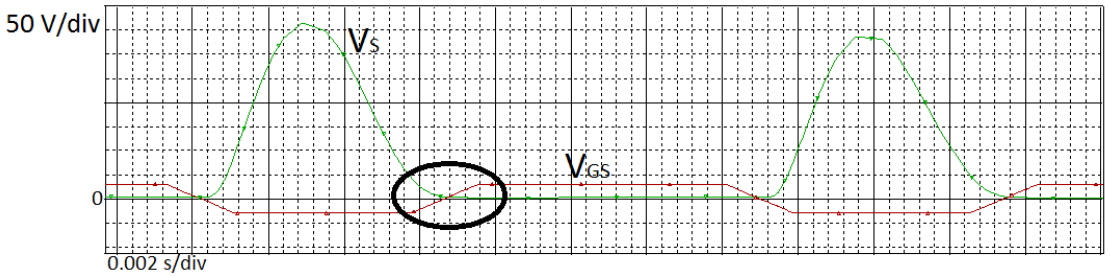

Figure 4.5 – Drain-Source Voltage Waveform with C_1 Tuned

Figure 4.6 shows the output voltage and current from the inverter. They are sinusoidal and have the desirable working frequency (13.57 Mhz, the same as the gate signal). The amplitudes can be compared with the theoretical equation. Simplifying equation (3.40) and (3.43) with the conditions of the simulation and using (3.40) in (3.43), the amplitude of the voltage is given by:

$$V_{Rim} = \frac{4V_I}{\sqrt{\pi^2 + 4}} \tag{4.8}$$

Simplifying equation (3.38) and using equation (3.48) on it, one can find the equation to the load's current amplitude:

$$I_{Rim} = \frac{8V_I}{(\pi^2 + 4)} \frac{1}{R_i} \frac{\sqrt{\pi^2 + 4}}{2} \tag{4.9}$$

The comparison of the results from the previous equations with the simulation show an absolute error of 2,2% for the voltage and 3,2% for the currents. These parameters are important for the design of the transmitter, because will allow to calculate the magnetic field created from the driver's antenna and the voltage generated in the transmitting coil.

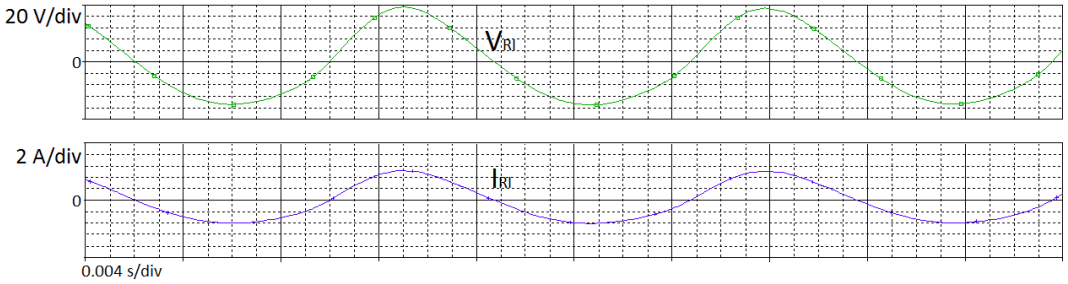

Figure 4.6 - Output Voltage and Current

The current source is kept direct by the choke inductor L_f with 10% maximum ripple. Figure 4.7 shows the comparison between the output current and the current source and since the ripple is minimal compared with the current at the load, the current at the source can be considered DC and the inductor is well designed. The value used for the choke inductor is a bit higher than the one calculated in (3.56) to ensure that the ripple is kept under 10%, that being $L_f = 12\mu H$.

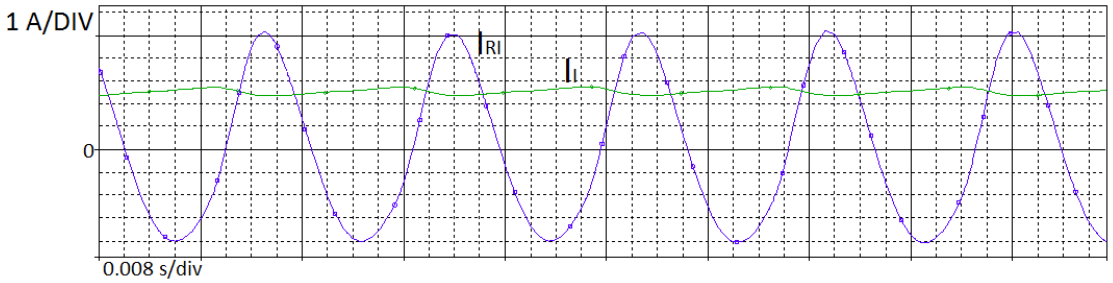

Figure 4.7 – Output Current and Source Current with $L_f = \mu H$

Considering the inductances and capacitors are ideal, the performance of the inverter is 95.6%. It is possible to enhance this value by changing the choke-inductor for a multi-resonant circuit, which will work as a harmonic filter. The result will be a reduced voltage stress on the MOSFET. This alteration makes the inverter almost become a class-F inverter, making the design significantly more complex, so it was not considered for this work.

4.3 – Antenna Inductance

A small driver's antenna is considered for the simulation, but it can be scaled according to the transmitting antenna. Its parameters are:

R_M	0.13 m
N	2 turns
C_D	2.54 mm
T_s	0.01 m

Using the technic described in the previous chapter, the self-inductance is calculated and its physical shape can be seen in Figure 4.8. The calculated value is:

L_{a1}	3.822 µH

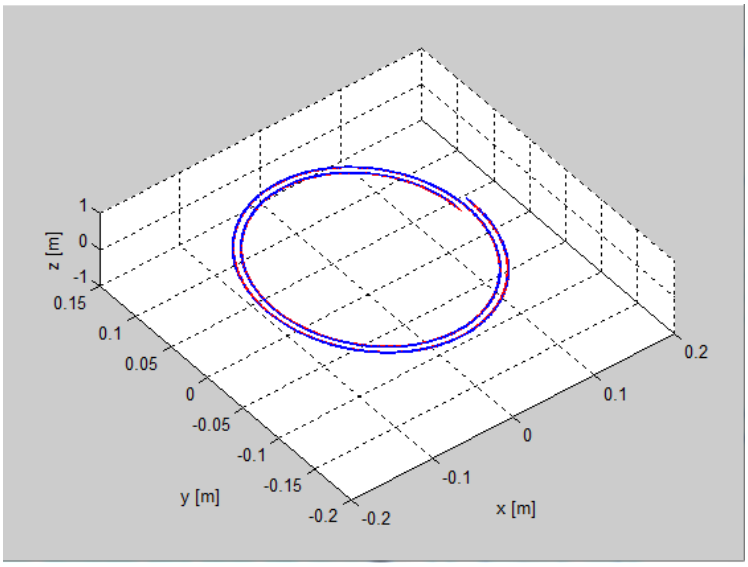

Figure 4.8 - Driver's antenna

The mix of both colors are consequence of the driver's coil and sensing coil almost overlapping.

In experimental settings, this value can be greatly affected by external influences and is recommended to be measured after the construction of the antenna.

The mutual inductance will influence the overall inductance of the antenna, because of the strong coupling between the coils. This difference can be later compensated by the matching circuit as well.

4.4 – Tuning C_2 and C_3

The values calculated with equations (3.62) and (3.63) are approximations from more complexes equations and equivalent circuits, therefor these values have some error, therefor to achieve the better results it is necessary to tune the capacitors.

Following [26], it is possible to tune the components graphically by analyzing the waveform of the voltage across the switch, recognize the load characteristics (amplitude and phase) and change the capacitors values accordantly. According to [26], the load's angle for optimum operation must be between about 40º and 70º and its resistance can only have variations of +55% and -33%. Figure 4.9 shows the waveform of the voltage across the switch with the values of the capacitors calculated with (3.62) and (3.63).

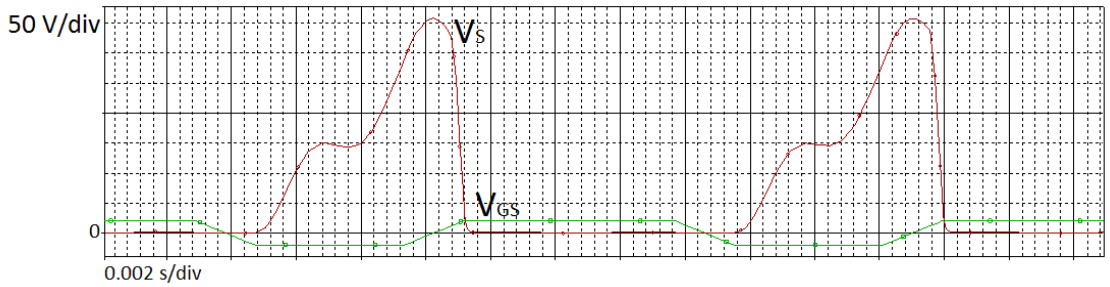

Figure 4.9 - Drain-Source Voltage Waveform with untuned matching circuit; $C_2 = 55.15pF$, $C_3 = 6pF$

It is possible to conclude that the inverter is not operating in optimum conditions, so the capacitors must be retuned. Altering C_2 will transform the amplitude and the phase of the load and C_3 will transform only the phase. The order for tuning then is to modify the load with C_2 and adjust the phase with C_3. The results of these adjustments can be seen in figure 4.10 and figure 4.11.

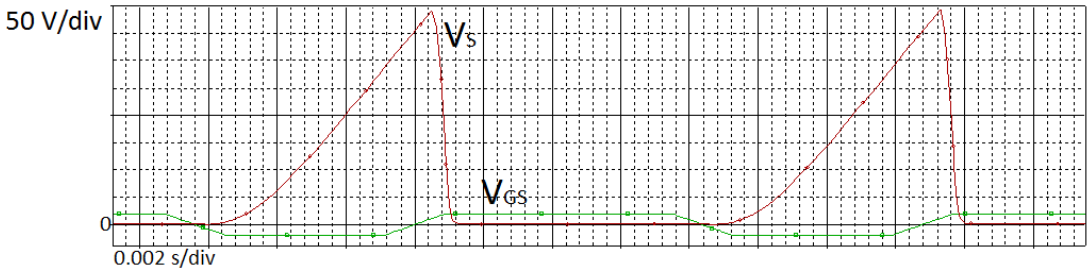

Figure 4.10 – Example for when the load resistance is out of the limits

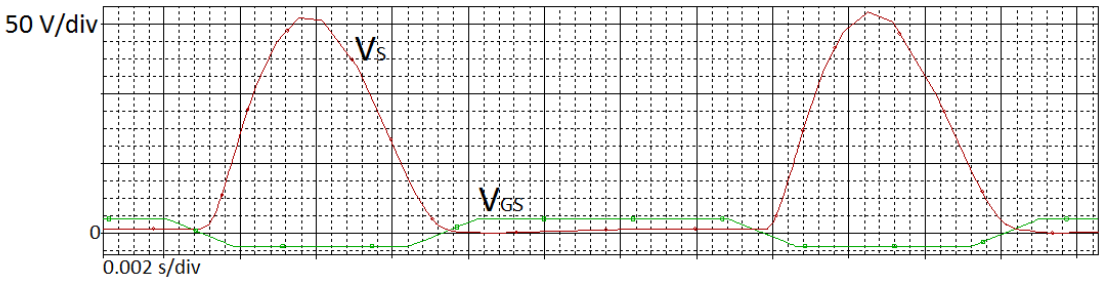

Figure 4.11 - Drain-Source Voltage Waveform with tuned matching circuit; $C_2 = 28$, $C_3 = 1pF$

The complete driver circuit is represented in figure 4.12, with the calculated components values to operate in optimum conditions.

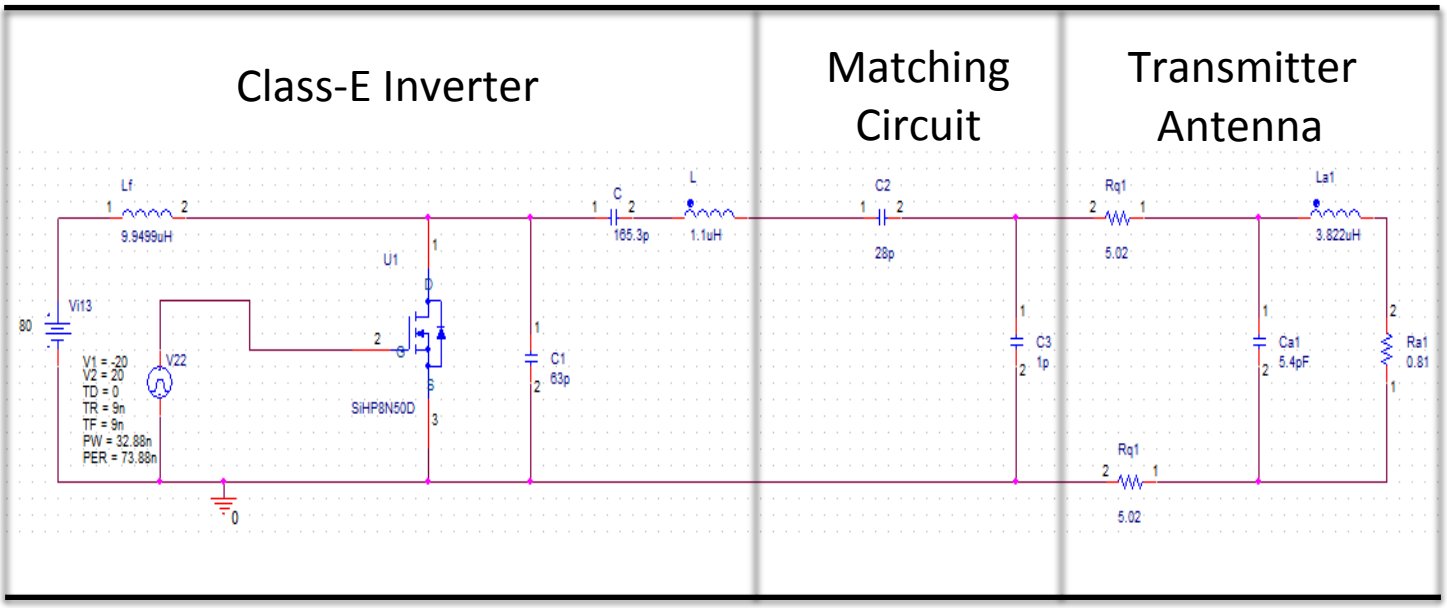

Figure 4.12 – Complete Driver Circuit

Chapter 5
Conclusions

5.1 Final Conclusion

A new way to explore power transferring wirelessly using the principle of evanescent waves opened new possibilities to free electronic devices from cables. This advances are already leading people to experiment and find the limits of this method. [24] [25] [26]

The technics presented here rely on a circuit to excite the system and an inverter made out of a Class-E inverter was purposed. This topology offers everything necessary to the resonant system:

1. Possibility to work at high frequencies, within the legal band ranges for radio frequencies;
2. Flexibility when choosing the output power and voltage. Because of the simplicity of the Class-E inverter, the components values can be recalculated to adjust to the desirable parameters;
3. The efficiency is also guarantee by the ZVS operation, regardless of the output power, which is not true when compared to other more common topologies.

The simulation presented in chapter 3 has the output power of 200W, which resulted in reasonable components values. Considering that many experiments transferred power wirelessly with an efficiency of around 70% at a distance of 1 meter, this solution can be used to supply energy to power a common electronic device, such as a cellphone or tablet.

However, the main drawback is the load sensibility. The advantages can only be guarantee if the value of input load is the one calculated with equation (3.45), which has a resistive only value. This is a problem, because the input impedance is complex due to the coils. To surpass this, a parallel-series, using only capacitors, matching circuit was designed to alter the profile of the load, as seen from the inverter. In the simulation results it is possible to see how the antenna impedance was converted and matched to the ideal load value for optimum operation. This solution offers major advantages when designing the driver's antenna, because can adapt to different values of inductance and loads. Although, some other topologies and calculations methods can work better for different ranges of inductances values.

An Archimedean shaped antenna was designed for simulation purposes only. The method presented in chapter 3 to calculate the inductance value can be used to calculate the antenna's self-inductance of any size. The calculated value should be used for reference only though, because the real value of any coil is hard to predict, using any

method. Therefore, the inductance must be measured after the antenna fabrication and recalculate the values of the rest of the components of the driver's circuit.

The Class-E inverter offers a relative high output power with high frequencies. It is not complex to design, giving flexibility to work with different input voltage, output power and operating frequency. When the matching circuit is properly tuned, it has high efficiency due to the ZVS.

5.2 Future Work

This thesis serves as a foundation ground to experiment such technic. It presents an efficient way to excite the resonant at fixed frequency and high output power, so naturally the next step is to set up the resonant system and test with the driver circuit. This work also introduces the Coupled Mode Theory, which is a base to analyze the problem in a physics perspective. A Further study to better understand all the elements that affect the system is of great interest. Many studies try different shape antennas [27] [28], but not in this context. Maybe different antenna's configuration would improve the system.

Since this is just the beginning, many improvements can be done in the inverter. Other, more complex, types of high frequency inverter are being developed [29] , such as the $\frac{}{2}$, that reduces the voltage stress in the MOSFET. This allows a much broader choice of MOSFET, because a MOSFET with higher maximum voltage, naturally has a bigger C_{out} capacitance, which make many models improper for the inverter. Working in high frequencies draws losses from conductors, because of the sky effect and reduces the efficiency of the overall system. Although expensive, litz wires are a great option for reducing such losses. There are many options for matching circuits to adapt the driver's antenna do the Class-E. Experiment different topologies to achieve less sensible components values would be a big improvement. For a more advance stage, a dynamic self-adaptive matching circuit could make the system in a situation where multiple devices are moving.

Appendix

Appendix A – Driver's components calculation

```
clc;
clear;

%Class-E components

%Paramentos de inicialização
Vi=80;
Primax=200;
f=13.56e6;
w=2*pi*f;
D=0.5;
Ql=5; %com 5 é quando funciona sempre
Coss_mosfet=52e-12;%SiHP8N50D
k=0.05;

%cálculo dos elementos do circuito

Ri=(8/(pi^2+4))*((Vi^2)/Primax)%resistencia da carga

L=Ql*Ri/(2*pi*f) %indutancia do tanque ressonante

Ctotal=8/(pi*(pi^2+4)*2*pi*f*Ri); %condensador em paralelo

C=1/(2*pi*f*Ri*(Ql-((pi*(pi^2-4))/16))) %condensador do tanque
ressonante

Lf=2*(((pi^2)/4)+1)*(Ri/f)

C1p = Ctotal-Coss_mosfet

Z=i*L-i*(1/C); %Reactance of the Class-E resonant tank

Ii=((Vi*8)/(pi^2+4))*(1/Ri); %corrente da fonte
Im=Ii*(sqrt(pi^2+4)/2) %amplitude da corrente na carga


%-------------------- Antenna Parameters-----------

fa=30e6; %antenna's resonant frequency must be above the system
frequency so the antenna can be seen as a inductive load from the
inversor
wa=2*pi*fa;
Qa=400; %quality factor to determine antenna's resistance, must be
30(+-10%)
Qt=30; %Target Quality factor(Antenna or system?)

La=(3.86)*10^-6; %approximate inductance calculated from the antenna
design

Ct=1/(wa^2*La)
```

```
Ct1=40.458e-12-Ct;

Ra=(w*La)/Qa

%-----------------------------------------------------------------------

Rq=0.5*(((w*La)/Qt)-Ra) %if necessary, put Rq resistance in each side
of the antenna to achive Qa=30(+-10%)

%Rq=0;

Rpa=((w*La)^2)/(Ra+2*Rq);

Lpa=La;

Cpa=Ct;

Rtr=Ri; %Juntar dois arquivos

%Rtr=18.5; %Value of resistance to match (design from the Class-E)

Xtr=imag(Z);
%Xtr=22; %Value of reactance to match (L and C of the resonant tank
(in series))

C1=1/(w*(sqrt(Rtr*Rpa/4))+(Xtr/2))   %change   the   magnitude   of   the
load(needs to be adjusted after calculated)
                                  %decreasing    C1    ->    increasing
antennas's Current

C2=(1/(w^2*(Lpa/2)))-(1/(w*sqrt((Rtr*Rpa)/4)))-2*Cpa    %%change    the
phase of the load(needs to be adjusted after calculated)
                                                      %if      C1      is
adjusted, C2 must be adjusted one more time to garantee ZVS
Ii=((Vi*8)/(pi^2+4))*(1/Ri); %corrente da fonte
Im=Ii*(sqrt(pi^2+4)/2); %amplitude da corrente na carga para o cálculo
da indutancia da antenna
Im_ef=Im/sqrt(2);
```

Appendix B – Antenna's inductance Calculation

```
function [P,dL] = spirals(type,Rm,RM,s,N,Nsteps,h)
%
%   type:   1 - Archimedeans
%           2 - Logaritmic
%           3 - Rectilinear

switch type
    case 'A' %Archimedean
    phi = linspace(0,2*N*pi,Nsteps);
    r = (1/(2*N*pi))*(RM-Rm)*phi + Rm - s;
    x = r.*cos(phi);
    y = r.*sin(phi);
    z = h*ones(1,Nsteps);
    P = [x' y' z'];
    dL = diff(P);
    dL = [ dL ; dL(size(dL,1),:)];
case 'B' %Bernoulli
    %r=a*exp(b*teta)
    a = Rm;
    b = log(RM/Rm)/(2*N*pi);
    phi = linspace(0,2*N*pi,Nsteps);
    r = a*exp(b*phi) - s;
    x = r.*cos(phi);
    y = r.*sin(phi);
    z = h*ones(1,Nsteps);
    P = [x' y' z'];
    dL = diff(P);
    dL = [ dL ; dL(size(dL,1),:)];
case 'R' %Rectilinear
    Ns = Nsteps/N; %numero de pontos por espira
    Nsl = ceil(Ns/4); %numero de pontos por lado da espira
    d = (RM-Rm)/ (N);
    x=[];
    y=[];
    for i =  1 : N
        y1 = linspace(-(Rm+i*d),(Rm+i*d),Nsl);
        x1 = (Rm+i*d)*ones(1,Nsl);
        y2 = (Rm+i*d)*ones(1,Nsl);
        x2 = linspace((Rm+i*d),-(Rm+i*d),Nsl);
        y3 = linspace((Rm+i*d),-(Rm+i*d)-d,Nsl);
        x3 = -(Rm+i*d)*ones(1,Nsl);
        y4 = -((Rm+i*d)+d)*ones(1,Nsl);
        x4 = linspace(-(Rm+i*d),(Rm+i*d)+d,Nsl);
        x = [x [x1 x2 x3 x4] ];
        y = [y [y1 y2 y3 y4] ];
    end
    z = h*ones(1,size(x,2));
    P = [x' y' z'];
    dL = diff(P);
    dL = [ dL ; dL(size(dL,1),:)];
end
```

```
clear all
close all
clc

N = 2; %Number of turns
ra=0.13; %Outer Antenna Radius
da=ra*2; %Outer Antenna Diameter
rc=0.00127; %Conductor Radius
dc=rc*2;%(2.54mm) %Conductor Diameter
Ts=0.01; %(1 cm) Spacing Between Turns

coil_type = 'A';
%RM = 0.295/2;
%Rm = 0.295/2-(0.00254+6*(0.01+0.00254));

RM = ra %This is the right side of the conductor on the last turn, so
the space of the conductor doesn't count
Rm = RM-(N*dc+(N-1)*Ts) %This is the left side of the conductor on the
first turn
%N = 2;
s =0.00015 %subtrai o valor de raio da antenna, para indutancia mutual
o valor deve ser zero
Nsteps = 1000;
z=0.01%para bater bem com o artigo 0.1/100; %alterado para bater bem
com o artigo
[P1 dL1] = spirals(coil_type,Rm,RM,0,N,Nsteps,0);
[P2 dL2] = spirals(coil_type,Rm,RM,s,N,Nsteps+1,0);

%Calculo do potencial vector
size_P1 = size(P1,1);
size_P2 = size(P2,1);
A = zeros(size_P2,3);
for i = 1 : size_P2
    D2 = ( repmat(P2(i,:),size_P1,1) - P1 ).^2; %quadrado da distancia
de cada componente de um ponto P2 a cada ponto de P1
    D = sqrt( sum(D2,2) ); % Distancia de cada P2 a todos os P1
%    ind=find(D<0.00001);
%    D(ind)=0.00001;
    dA = dL1./repmat(D,1,3);
    A(i,:) = sum(dA,1);
end
figure
quiver3(P1(:,1), P1(:,2), P1(:,3), dL1(:,1), dL1(:,2), dL1(:,3))
xlabel('x [m]')
ylabel('y [m]')
zlabel('z [m]')
hold on
quiver3(P2(:,1), P2(:,2), P2(:,3), A(:,1), A(:,2), A(:,3),'-.r')
view(-45,45)
drawnow

%Calculo da indutancia
L = sum(sum(A.*dL2))/7.5 % uH , divided by the current ABS value
```

Appendix C – MOSFET's Datasheet

VISHAY
www.vishay.com

SiHP8N50D
Vishay Siliconix

D Series Power MOSFET

PRODUCT SUMMARY		
V_{DS} (V) at T_J max.	550	
$R_{DS(on)}$ max. at 25 °C (Ω)	V_{GS} = 10 V	0.85
Q_g (max.) (nC)	30	
Q_{gs} (nC)	4	
Q_{gd} (nC)	7	
Configuration	Single	

FEATURES
- Optimal Design
  - Low Area Specific On-Resistance
  - Low Input Capacitance (C_{iss})
  - Reduced Capacitive Switching Losses
  - High Body Diode Ruggedness
  - Avalanche Energy Rated (UIS)
- Optimal Efficiency and Operation
  - Low Cost
  - Simple Gate Drive Circuitry
  - Low Figure-of-Merit (FOM): $R_{on} \times Q_g$
  - Fast Switching
- Material categorization: For definitions of compliance please see www.vishay.com/doc?99912

RoHS COMPLIANT
HALOGEN FREE Available

TO-220AB

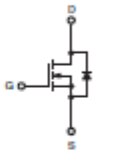

N-Channel MOSFET

APPLICATIONS
- Consumer Electronics
  - Displays (LCD or Plasma TV)
- Server and Telecom Power Supplies
  - SMPS
- Industrial
  - Welding
  - Induction Heating
  - Motor Drives
- Battery Chargers

ORDERING INFORMATION	
Package	TO-220AB
Lead (Pb)-free	SiHP8N50D-E3
Lead (Pb)-free and Halogen-free	SiHP8N50D-GE3

ABSOLUTE MAXIMUM RATINGS (T_C = 25 °C, unless otherwise noted)

PARAMETER			SYMBOL	LIMIT	UNIT
Drain-Source Voltage			V_{DS}	500	V
Gate-Source Voltage			V_{GS}	± 30	
Gate-Source Voltage AC (f > 1 Hz)				30	
Continuous Drain Current (T_J = 150 °C)	V_{GS} at 10 V	T_C = 25 °C	I_D	8.7	A
		T_C = 100 °C		5.5	
Pulsed Drain Current[a]			I_{DM}	18	
Linear Derating Factor				1.25	W/°C
Single Pulse Avalanche Energy[b]			E_{AS}	29	mJ
Maximum Power Dissipation			P_D	156	W
Operating Junction and Storage Temperature Range			T_J, T_{stg}	- 55 to + 150	°C
Drain-Source Voltage Slope	T_J = 125 °C		dV/dt	24	V/ns
Reverse Diode dV/dt[d]				0.37	
Soldering Recommendations (Peak Temperature)[c]	for 10 s			300	°C

Notes
a. Repetitive rating; pulse width limited by maximum junction temperature.
b. V_{DD} = 50 V, starting T_J = 25 °C, L = 2.3 mH, R_g = 25 Ω, I_{AS} = 5 A.
c. 1.6 mm from case.
d. $I_{SD} \leq I_D$, starting T_J = 25 °C.

For technical questions, contact: hvm@vishay.com
THIS DOCUMENT IS SUBJECT TO CHANGE WITHOUT NOTICE. THE PRODUCTS DESCRIBED HEREIN AND THIS DOCUMENT ARE SUBJECT TO SPECIFIC DISCLAIMERS, SET FORTH AT www.vishay.com/doc?91000

THERMAL RESISTANCE RATINGS				
PARAMETER	SYMBOL	TYP.	MAX.	UNIT
Maximum Junction-to-Ambient	R_{thJA}	-	62	°C/W
Maximum Junction-to-Case (Drain)	R_{thJC}	-	0.8	

SPECIFICATIONS (T_J = 25 °C, unless otherwise noted)

PARAMETER	SYMBOL	TEST CONDITIONS	MIN.	TYP.	MAX.	UNIT
Static						
Drain-Source Breakdown Voltage	V_{DS}	V_{GS} = 0 V, I_D = 250 µA	500	-	-	V
V_{DS} Temperature Coefficient	$\Delta V_{DS}/T_J$	Reference to 25 °C, I_D = 250 µA	-	0.58	-	V/°C
Gate-Source Threshold Voltage (N)	$V_{GS(th)}$	V_{DS} = V_{GS}, I_D = 250 µA	3	-	5	V
Gate-Source Leakage	I_{GSS}	V_{GS} = ± 30 V	-	-	± 100	nA
Zero Gate Voltage Drain Current	I_{DSS}	V_{DS} = 500 V, V_{GS} = 0 V	-	-	1	µA
		V_{DS} = 400 V, V_{GS} = 0 V, T_J = 125 °C	-	-	10	
Drain-Source On-State Resistance	$R_{DS(on)}$	V_{GS} = 10 V; I_D = 4 A	-	0.70	0.85	Ω
Forward Transconductance[a]	g_{fs}	V_{DS} = 20 V, I_D = 4 A	-	3	-	S
Dynamic						
Input Capacitance	C_{iss}	V_{GS} = 0 V, V_{DS} = 100 V, f = 1 MHz	-	527	-	pF
Output Capacitance	C_{oss}		-	52	-	
Reverse Transfer Capacitance	C_{rss}		-	8	-	
Effective Output Capacitance, Energy Related[b]	$C_{o(er)}$	V_{DS} = 0 V to 400 V, V_{GS} = 0 V	-	46	-	
Effective Output Capacitance, Time Related[c]	$C_{o(tr)}$		-	64	-	
Total Gate Charge	Q_g	V_{GS} = 10 V; I_D = 4 A, V_{DS} = 400 V	-	15	30	nC
Gate-Source Charge	Q_{gs}		-	4	-	
Gate-Drain Charge	Q_{gd}		-	7	-	
Turn-On Delay Time	$t_{d(on)}$	V_{DD} = 400 V, I_D = 4 A, R_g = 9.1 Ω, V_{GS} = 10 V	-	13	26	ns
Rise Time	t_r		-	16	32	
Turn-Off Delay Time	$t_{d(off)}$		-	17	34	
Fall Time	t_f		-	11	22	
Gate Input Resistance	R_g	f = 1 MHz, open drain	-	1.8	-	Ω
Drain-Source Body Diode Characteristics						
Continuous Source-Drain Diode Current	I_S	MOSFET symbol showing the integral reverse p - n junction diode 	-	-	8	A
Pulsed Diode Forward Current	I_{SM}		-	-	32	
Diode Forward Voltage	V_{SD}	T_J = 25 °C, I_S = 4 A, V_{GS} = 0 V	-	-	1.2	V
Reverse Recovery Time	t_{rr}	T_J = 25 °C, I_F = I_S = 4 A, dI/dt = 100 A/µs, V_R = 20 V	-	308	-	ns
Reverse Recovery Charge	Q_{rr}		-	1.8	-	µC
Reverse Recovery Current	I_{RRM}		-	11	-	A

Notes

a. Repetitive rating; pulse width limited by maximum junction temperature.
b. $C_{o(er)}$ is a fixed capacitance that gives the same energy as C_{oss} while V_{DS} is rising from 0 % to 80 % V_{DSS}.
c. $C_{o(tr)}$ is a fixed capacitance that gives the same charging time as C_{oss} while V_{DS} is rising from 0 % to 80 % V_{DSS}.

For technical questions, contact: hvm@vishay.com
THIS DOCUMENT IS SUBJECT TO CHANGE WITHOUT NOTICE. THE PRODUCTS DESCRIBED HEREIN AND THIS DOCUMENT ARE SUBJECT TO SPECIFIC DISCLAIMERS, SET FORTH AT www.vishay.com/doc?91000

Bibliography

[1] C. Mendes, Inductive Link - doctoral thesis, 2012.

[2] N. Tesla, "Apparatus for Transmission of Electrical Energy," *Patent*, no. US 649621 A, 1900.

[3] M. Hunsicker, "The Future of Wireless Charging: Ubiquitous Technology Will Enable Anytime, Anywhere Recharding," in *The Image Sensors 2009 Wireless Power Submmit*, San Diego, CA, 2009.

[4] S. Sasaki, K. Tanaka and K.-I. Maki, "Microwave Power Transmission Technologies for Solar Power Satelites," *IEEE Trans. Power Electron.*, vol. 101, no. 6, June 2013.

[5] A. Kurs, "Power Transfer Through Strongly Coupled Resonances," *MIT Thesis*, September 2007.

[6] A. P. Sample, D. A. Meyer and J. R. Smith, "Analysis, Experimental Results and Range Adaptation of Magnetically Couple Resonators for Wireless Power Transfer," *IEEE Transactions on Industrial Electronics*, vol. 58, no. 2, February 2011.

[7] A. Karalis, J. D. Joannopoulos and M. Soljačić, "Efficient Wireless non-raduatuve Mid-Range Energy Transfer," *Annals of Physics 2008*, vol. 27, pp. 34-38, April 2007.

[8] "International Commission on Non-Ionizing Radiation Protection. Guidelines for limiting exposure to time-varying electric, magnetic, and electromagnetic fields (up to 300 GHz).," *Health Phys*, vol. 74, p. 494 –522, 1998.

[9] "Radio Regulations," ITU-R, Edition 2012.

[10] A. Inoue, T. Heima, A. Ohta and R. Hattori, "Analysis of class-F and inverse class-F amplifiers," *Microwave Symposium Digest. IEEE MTT-S International*, vol. 2, 2000.

[11] M. K. Kazimierczuk and K. Puczko, Resonant Power Converter, Second Edition.

[12] "AN11019, Antenna Design Guide," NXP Semiconductors, July 2012.

[13] F. H. Raab, "Effects of Circuit Variations on the Class-E Tuned Power Amplifier,"

IEEE Journal of Solid-State Circuits, vol. 3, April 1978.

[14] Y. OZAWA and T. Naohiro, "Study of Electric Aircraft Charged by Beamed Microwave Power," *IHI Engineering Review,* vol. Vol. 48, no. No. 2, 2015.

[15] P. E. Glaser, "Power from the Sun: Its Future," *Science,* vol. Volume 162, p. Page 857, 1968.

[16] C. A. Balanis, Antenna Theory: Analysis and Design, Wiley-Interscience, 2005.

[17] K. Finkenzeller, RFID Handbook, Wiley, 2010.

[18] T. Imura and Y. Hori, "Maximizing Air Gap and Efficiency of Magnetic Resonant Coupling for Wireless Power Transfer Using Equivalent Circuit and Neumann Formula," *IEEE TRANSACTIONS ON INDUSTRIAL ELECTRONICS,* vol. Vol. 58, 2011.

[19] Z. N. Low, R. A. Ching, R. Tseng and J. Lin, "Design and Test of a High-Power High-Efficiency Loosely Coupled Planar Wireless Power Transfer System," *IEEE TRANSACTIONS ON INDUSTRIAL ELECTRONICS,* vol. Vol. 56, 2009.

[20] T. Beh, M. Kato, T. Imura and Y. Hori, "Wireless Power Transfer System via Magnetic Resonant Coupling at Fixed Resonance Frequency -Power Transfer System Based on Impedance Matching -," *World Electric Vehicle Journal,* vol. Vol. 4, 2010.

[21] K. Hee-Seung, W. Do-Hyun and J. Byung-Jun, "Simple design method of wireless power transfer system using 13.56MHz loop antennas," *IEEE.*

[22] K. Fotopoulou and B. W. Flynn, "Wireless Power Transfer in Loosely Coupled Links, Coil Misalignment Model," *IEEE TRANSACTIONS ON MAGNETICS,* vol. Vol. 47, 2011.

[23] A. B. o. M. R. Safety.

[24] J. M. Rivas, Y. Han, O. Leitermann, A. Sagneri and D. J. Perreault, "A High-Frequency Resonant Inverter Topology with Low Voltage Stress".

[25] Z. Fengfan, "Wireless Power Transfer Based on Double Loop Antennas".

[26] J. Uei-Ming, "Design and Optimization of Printed Spiral Coils for Efficient Transcutaneous Inductive Power Transmission," *IEEE TRANSACTIONS ON BIOMEDICAL CIRCUITS AND SYSTEMS,* vol. Vol. 1, 2007.

[27] J. RAIMAN, "SENIOR THESIS: WIRELESS ELECTRICITY AND IMPEDANCE MATCHING," 2013.

[28] "Analysis, Experimental Results, and Range Adaptation of Magnetically Coupled Resonators for Wireless Power Transfer," *IEEE TRANSACTIONS ON INDUSTRIAL ELECTRONICS*, vol. Vol. 58, 2011.

[29] J. Markoff, ""Intel Moves to Free Gadgets of Their Recharging Cords"," NY Times, 2008.

[30] A. Kurs, A. Karalis, R. Moffatt, J. D. Joannopoulos, P. Fisher and M. Soljacic, "Wireless Power Transfer via Strongly Coupled Magnetic Resonances," *SCIENCE*, vol. VOL. 317, 2007.

[31] T. Aoki, B. Dayan, E. Wilcut, W. P. Bowen, A. S. Parkins, T. J. Kippenberg, K. J. Vahala and H. J. Kimble, "Observation of strong coupling between one atom and a monolithic microresonator," *Nature*, 2006.

[32] H. A. Haus, Waves and Fields in Optoeletronics, Prentice-Hall, 1984.

[33] C.-S. Wang, O. H. Stielau and G. A. Covic, "Design Considerations for a Contactless Electric Vehicle Battery Charger," *IEEE TRANSACTIONS ON INDUSTRIAL ELECTRONICS,*, vol. VOL. 52, 2005.

[34] N. Hanbiao and L. Jianhui, "Design of Loosely Coupled Inductive Power Transfer Systems for Instrumented Wheelset," in *The Ninth International Conference on Electronic Measurement & Instruments*, 2009.

[35] V. G. Krizhanovsk, D. V. Chernov and M. K. Kazimierczuk, "Low-Voltage Self-Oscillating Class E Electronic Ballast for Fluorescent Lamps," *ISCAS*, 2006.